

# Hopf Bifurcation of Spike Solutions for the Shadow Gierer-Meinhardt Model

M. J. WARD, and J. WEI

*Michael Ward: Department of Mathematics, University of British Columbia, Vancouver, Canada V6T 1Z2, Juncheng Wei: Department of Mathematics, Chinese University of Hong Kong, Shatin, New Territories, Hong Kong*

(Received 30 March 2002)

In the limit of small activator diffusivity, the stability of a one-spike solution to the shadow Gierer-Meinhardt activator-inhibitor system is studied for various ranges of the reaction-time constant  $\tau$  associated with the inhibitor field dynamics. By analyzing the spectrum of the eigenvalue problem associated with the linearization around a one-spike solution, it is proved, for a certain parameter regime, that a complex conjugate pair of eigenvalues crosses into the unstable right half-plane  $\text{Re}(\lambda) > 0$  as  $\tau$  increases past a critical value  $\tau_0$ . For this parameter regime, it is proved that there are exactly two eigenvalues in the right half-plane when  $\tau > \tau_0$  and none when  $0 \leq \tau < \tau_0$ . It is shown numerically that this critical value of  $\tau$  represents the onset of an oscillatory instability in the height of the spike. For other parameter regimes, a similar Hopf bifurcation is confirmed numerically. Full numerical solutions to the shadow problem are computed for a spike that is initially centred at the origin of a radially symmetric domain. Different types of large-scale oscillatory motions for the height of a spike are observed numerically for values of  $\tau$  well beyond  $\tau_0$ .

## 1 Introduction

The Gierer-Meinhardt (GM) model, introduced in [8], is a reaction-diffusion system of activator-inhibitor type. It has been widely used to model localization processes in nature, such as cell differentiation and morphogenesis (cf. [10]), biological pattern formation (cf. [15]), and the formation of sea-shell patterns (cf. [16]). In dimensionless form, the GM model is given by

$$a_t = \varepsilon^2 \Delta a - a + \frac{a^p}{h^q}, \quad x \in \Omega, \quad t > 0, \quad (1.1 a)$$

$$\tau h_t = D \Delta h - \mu h + \frac{a^m}{h^s}, \quad x \in \Omega, \quad t > 0, \quad (1.1 b)$$

$$\partial_n a = \partial_n h = 0, \quad x \in \partial\Omega. \quad (1.1 c)$$

Here  $a, h, D > 0$ ,  $0 < \varepsilon \ll 1$ ,  $\mu > 0$  and  $\tau \geq 0$  represent the activator concentration, inhibitor concentration, inhibitor diffusivity, activator diffusivity, inhibitor decay rate, and reaction-time constant, respectively. The parameters  $D, \varepsilon, \mu$  and  $\tau$  are assumed to be constant, and the domain  $\Omega \in \mathbb{R}^N$  is bounded. The usual assumption on the exponents  $(p, q, m, s)$  (cf. [8]) are that they satisfy

$$1 < p < p_c, \quad q > 0, \quad m > 1, \quad s \geq 0, \quad \text{with} \quad \zeta \equiv \frac{qm}{(p-1)} - (s+1) > 0. \quad (1.2)$$

Here  $p_c$  is the critical Sobolev exponent for  $\mathbb{R}^N$ , with  $p_c = 5$  for  $\mathbb{R}^3$ .

The GM model exhibits surprisingly rich dynamics for various parameter ranges. For  $\varepsilon \ll 1$ , the GM model exhibits a Turing instability (cf. [21]), whereby small amplitude spatially varying states undergo an instability to larger amplitude spatially inhomogeneous stationary states (cf. [8], [15]). Spatially inhomogeneous states where the activator concentration  $a$  is localized at discrete points in  $\mathbb{R}^N$  are referred to either as spot or spike-type patterns. Stripe patterns occur when  $a$  is localized along some  $\mathbb{R}^{N-1}$  dimensional manifold in  $\mathbb{R}^N$ . Both types of patterns have been observed, and have been studied numerically since the early 1970's (see [8], [10], [15], [16] and the references therein). However, from a mathematical viewpoint, there are many open problems that remain concerning the stability and dynamics of large amplitude solutions for (1.1).

The goal of this paper is to study oscillatory-type instabilities that occur for spike-type solutions of the limiting form of the GM model obtained by letting  $D \rightarrow \infty$  in (1.1 b). The resulting well-known system (cf. [24], [11], [3]), called the shadow GM model, is given by

$$a_t = \varepsilon^2 \Delta a - a + a^p/h^q, \quad x \in \Omega, \quad t > 0, \quad (1.3 a)$$

$$\partial_n a = 0, \quad x \in \partial\Omega, \quad (1.3 b)$$

$$\tau h_t = -\mu h + \frac{\varepsilon^{-N}}{|\Omega|} \int_{\Omega} \frac{a^m}{h^s} dx. \quad (1.3 c)$$

In (1.3 c),  $|\Omega|$  denotes the volume of  $\Omega$ .

In the limit  $\varepsilon \rightarrow 0$ , the existence of equilibrium spike-type solutions for (1.3) is now very well-understood. There can be boundary spikes whose support are on  $\partial\Omega$  (cf. [19]), and interior spikes located strictly inside  $\Omega$ . The determination of the equilibrium spike locations for interior spike solutions to (1.3) has been found to be related to certain geometric ball-packing problems (see [2], [9], [13], [22], [25], and the references therein). For the case  $\tau = 0$ , the dynamics and stability of interior spikes is also well-understood. For  $\tau = 0$ , and for certain ranges of the exponents  $m$  and  $p$ , and the dimension  $N$ , an interior one-spike equilibrium solution to (1.3) is unstable, but has an exponentially small growth rate as  $\varepsilon \rightarrow 0$ . This weak instability, known as metastability, results in an asymptotically exponentially slow drift of the spike towards the closest point on the boundary of  $\Omega$  (cf. [11], [11], [24]). When  $\tau = 0$ , the motion of a one-spike solution to (1.3) along the boundary of  $\Omega$  has also been characterized (cf. [12]). When  $\tau = 0$ , equilibrium solutions for (1.3) with two or more interior spikes are always unstable with an  $O(1)$  growth rate as  $\varepsilon \rightarrow 0$ .

In contrast, the instabilities that occur when  $\tau > 0$  are not well-understood. To illustrate the instability, we consider the unit ball in  $\mathbb{R}^2$  with a spike located at the origin. The resulting radially symmetric equilibrium solution  $a = a_e$  and  $h = h_e$ , computed numerically, is shown in Fig. 1(a). We then perturb this equilibrium solution for  $a$  slightly, with the form of the local perturbation described precisely in (5.2) of §5 below. Using this perturbation as the initial condition for  $a$ , and taking the unperturbed value  $h(0) = h_e$ , we then solve (1.3) dynamically for two values of  $\tau$ . In Fig. 1(b) we plot the resulting amplitude  $a_m$  of the spike as a function of time. The amplitude  $a_m$  is defined to be the value of  $a$  at the centre of the unit ball. From this figure, we see that for  $\tau = 0.53$  the initial perturbation dies out as  $t$  increases, whereas for  $\tau = 0.58$  an oscillatory instability is triggered. This suggests that there could be a Hopf bifurcation at some critical value

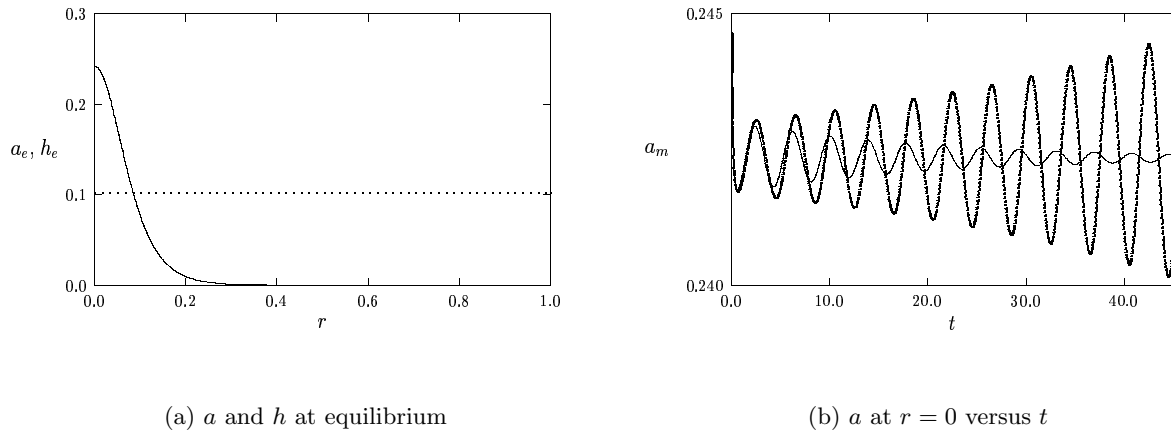


FIGURE 1. In the leftmost figure we plot the equilibrium  $a$  (solid curve) and  $h$  (dashed curve). In the rightmost figure we plot  $a$  at  $r = 0$  versus  $t$  for  $\tau = 0.53$  (solid curve) and  $\tau = 0.58$  (heavy solid curve). The exponent set is  $(p, q, m, s) = (2, 1, 2, 0)$ , with  $N = 2$ ,  $\varepsilon = 0.05$ , and  $\mu = 1$ .

$\tau_0$  between  $\tau = 0.53$  and  $\tau = 0.58$ . A numerical computation, that relies on our theoretical framework, gives  $\tau_0 = 0.561$ . The possibility of this type of instability was first observed in [18], where similar plots were shown for the exponent set  $(p, q, m, s) = (2, 1, 2, 0)$  with  $N = 1$ .

The main goal of this paper is study the instability of a one-spike solution to (1.3) as a function of the reaction-time constant  $\tau$ . In the limit  $\varepsilon \rightarrow 0$ , we linearize (1.3) around an interior one-spike solution to obtain a nonlocal eigenvalue problem, labeled by NLEP, that is independent of  $\varepsilon$ , of the location of the spike within  $\Omega$ , and of the shape of  $\Omega$ . The spectrum of this eigenvalue problem, which governs localized instabilities, is studied using a combination of analytical, asymptotic, and numerical techniques. The level of precision of our results depends on the exponent set  $(p, q, m, s)$  and the dimension  $N$ . We refer to data as being of Type 1 if  $(p, q, m, s)$  satisfy  $m = 2$  and  $1 < p \leq 1 + 4/N$ , in addition to the usual assumption (1.2). Type 2 data refers to exponent sets satisfying (1.2) and either  $m \neq 2$  or  $p > 1 + 4/N$ .

For Type 1 data, in §2 we prove in Theorem 2.3 that there is a unique value  $\tau = \tau_0 > 0$  for which the eigenvalue problem NLEP has a complex conjugate pair of eigenvalues  $\lambda = \pm i\lambda_I^0 \neq 0$  on the imaginary axis. A rigorous and accurate lower bound for  $\lambda_I^0$  is obtained in Lemma 2.5 of §2. The critical values  $\tau_0$  and  $\lambda_I^0$  for various exponent sets  $(p, q, m, s)$  and dimensions  $N$  are computed numerically in §3. In particular, for the exponent set of Fig. 1(b) we compute that  $\tau_0 = 0.561$ . In Lemma 3.1 of §3 we prove that as  $\tau$  increases past  $\tau_0$ , these two eigenvalues of NLEP have a strict transversality into the unstable right half-plane  $\text{Re}(\lambda) > 0$ . In Lemma 3.1, we use a winding number argument to prove that when  $\tau > \tau_0$ , there are exactly two eigenvalues of NLEP in the right half-plane. Alternatively, when  $0 \leq \tau < \tau_0$ , there are no eigenvalues of NLEP in the right half-plane. Thus, we have a Hopf bifurcation. In §3 we show that there is another critical value  $\tau = \tau_c$  at which the two complex conjugate eigenvalues merge onto the positive real axis at  $\lambda = \lambda_R^0$ . Values for the

critical parameters  $\tau_c$  and  $\lambda_R^0$  are computed numerically. For  $\tau > \tau_c$ , the eigenvalues are shown to remain along the positive real axis, and their movement along the real axis as a function of  $\tau$  is tracked.

For Type 2 data, our analytical results are weaker. Under a certain monotonicity condition, which must be verified numerically for each exponent set  $(p, q, m, s)$  and dimension  $N$ , in §4 we show that the results obtained for Type 1 data also largely apply for Type 2 data. Under this monotonicity condition, there is a unique value  $\tau_0$  at which a pair of complex conjugate pair of eigenvalues cross the imaginary axis at  $\lambda = \pm i\lambda_I^0 \neq 0$ . For  $\tau > \tau_0$ , there are two eigenvalues in the right half-plane, and they merge onto the positive real axis at  $\lambda = \lambda_R^0 > 0$  at some  $\tau = \tau_c > \tau_0$ . They remain on the real axis for any  $\tau > \tau_c$ . The key difference here is that it is possible that  $\tau_0 < 0$  and  $\tau_c < 0$ . This implies that there can be an instability already present when  $\tau = 0$ . For the typical exponent sets used previously for the GM model ([8], [10], [15], and [16]), we have verified numerically that our monotonicity assumption is satisfied. For these exponent sets, in §4 we compute numerical values for  $\tau_0$ ,  $\tau_c$ ,  $\lambda_I^0$  and  $\lambda_R^0$ . We were unable to construct an exponent set  $(p, q, m, s)$  and dimension  $N$  where our monotonicity condition is violated. Whether this condition is always satisfied is an open problem.

There have been only a few previous works to characterize the spectrum of the linearization of (1.3) around a one-spike solution. In [20], under the key assumption that the exponent set  $(p, q, m, s)$  is such that  $\zeta \rightarrow 0^+$  in (1.2), many stability and instability results were obtained for the one-dimensional case  $N = 1$ . Our results, however, apply for any  $\zeta > 0$  and dimension  $N$  satisfying (1.2). Thus, we can obtain stability and instability results for the exponent sets used in the numerical simulations of the GM model in [8], [10], [15], and [16]. Using a simple perturbation analysis for  $\zeta \rightarrow 0^+$ , we formally recover a result of [20] in §4. In [4] it is proved that there are two eigenvalues of the eigenvalue problem NLEP along the positive real axis when  $\tau$  is sufficiently large, and a Hopf bifurcation as  $\tau$  increases past some critical parameter is suggested.

Our approach to analyze the stability of a spike solution to (1.3) is related to the studies in [5], [6], and [7], of the stability of a one-spike solution to the Gray-Scott model. The behaviour of the spectrum of the linearization of the Gray-Scott model obtained in [6] is qualitatively very similar to what we have found for the spectrum of the linearization of (1.3). However, since these previous results for the Gray-Scott model rely on dynamical systems techniques, they are obtained only for the case of one spatial dimension. The analysis presented here is based on a PDE-type approach and, consequently, we are able to consider the effect of the dimension  $N$  on the stability of one-spike solutions to the shadow GM model.

In §5 we consider the full dynamics under (1.3) for a one-spike solution initially located at the centre of the unit ball in  $\mathbb{R}^N$ . We take  $\varepsilon \ll 1$ , and consider an initial condition for  $a$  that represents a small radially symmetric perturbation away from the equilibrium solution. For various exponent sets, we first verify that an oscillatory instability is triggered for  $\tau$  slightly beyond  $\tau_0$ . Then, for the common exponent set  $(p, q, m, s) = (2, 1, 2, 0)$ , with  $N = 1$  and  $N = 2$ , we investigate numerically the dynamical behaviour of (1.3) well after the initial instability has been triggered. Numerical results are shown for various values of  $\tau > \tau_0$ . A very complicated oscillatory motion for the amplitude of the spike as a function of time is obtained

when  $\tau_0 < \tau < \tau_c$ . This type of behaviour has not been noted previously. An attempt is made to explain this motion qualitatively.

## 2 Analytical Results for the Eigenvalue Problem

In this section we obtain some analytical results concerning the stability of a one-spike solution to (1.3). As shown in [11] and [24], a one-spike equilibrium solution  $a_\varepsilon, h_\varepsilon$  for (1.3) in the limit  $\varepsilon \rightarrow 0$  is given by

$$a_\varepsilon(x) \sim h_\varepsilon^\gamma w [\varepsilon^{-1}|x - x_0|], \quad \gamma = q/(p-1), \quad (2.1 a)$$

$$h_\varepsilon \sim \left( \frac{\varepsilon^{-N}}{\mu|\Omega|} \int_\Omega w^m dx \right)^{1/[1+s-\gamma m]} \sim \left( \frac{1}{\mu|\Omega|} \int_{\mathbb{R}^N} [w(|y|)]^m dy \right)^{1/[1+s-\gamma m]}, \quad (2.1 b)$$

for some  $x_0 \in \Omega$ . Here  $|\Omega|$  is the volume of  $\Omega$ ,  $y = \varepsilon^{-1}(x - x_0)$ , and  $w(\rho)$  satisfies the radially symmetric problem

$$w'' + \frac{(N-1)}{\rho} w' - w + w^p = 0, \quad \rho \geq 0, \quad (2.2 a)$$

$$w(0) > 0, \quad w'(0) = 0, \quad w \sim c\rho^{-(N-1)/2} e^{-\rho}, \quad \text{as } \rho \rightarrow \infty, \quad (2.2 b)$$

where  $c$  is a positive constant. There exists a unique solution to (2.2) when  $N = 1$  and  $N = 2$ , while for  $N = 3$  we require that  $p < p_c$ .

To determine the stability of this solution, we substitute  $a = a_\varepsilon + e^{\lambda t} \phi [\varepsilon^{-1}(x - x_0)]$  and  $h = h_\varepsilon + e^{\lambda t} \eta$  into (1.3), where  $\phi \ll 1$  and  $\eta \ll 1$ . Replacing the finite domain by the asymptotically infinite domain  $\varepsilon^{-1}\Omega$ , we obtain a nonlocal eigenvalue problem for  $\phi(y)$ ,

$$L_0 \phi - \frac{qm}{s+1+\frac{\tau\lambda}{\mu}} w^p \left( \frac{\int_{\mathbb{R}^N} w^{m-1} \phi dy}{\int_{\mathbb{R}^N} w^m dy} \right) = \lambda \phi, \quad -\infty < y < \infty, \quad (2.3 a)$$

$$\phi \rightarrow 0, \quad \text{as } |y| \rightarrow \infty, \quad (2.3 b)$$

where

$$L_0 \phi \equiv \Delta \phi - \phi + pw^{p-1} \phi. \quad (2.3 c)$$

The operator  $L_0$  is referred to as the local operator. Notice that (2.3) is independent of the shape of  $\Omega$ , of  $\varepsilon$ , and of the spike-layer location  $x_0$ . There are two key formulae related to  $L_0$  that are needed below. A direct calculation shows that

$$L_0^{-1} w^p = \frac{w}{p-1}; \quad L_0^{-1} w = \frac{w}{p-1} + \frac{1}{2} y \cdot \nabla w = \frac{w}{p-1} + \frac{1}{2} \rho w'. \quad (2.4)$$

The eigenvalue problem (2.3) is nonstandard for two reasons. It is nonlocal and the multiplier of the nonlocal term also depends on the eigenvalue  $\lambda$ . For the case  $N = 1$ , a similar eigenvalue problem was studied in [5], [6], and [7], in regards to the stability of a one-spike solution to the Gray-Scott model.

We now briefly review some known results on the spectrum of (2.3). The first result concerns the spectrum of the local operator  $L_0$  in (2.3 c).

**Theorem 2.1** (From [14]): *Consider the local eigenvalue problem  $L_0\phi_l = \nu\phi_l$  for  $\phi_l \in \mathcal{H}^1(\mathbb{R}^N)$ . This problem admits the eigenvalues  $\nu_0 > 0$ ,  $\nu_1 = \dots = \nu_N = 0$ , and  $\nu_{N+k} < 0$  for  $k \geq 1$ . The eigenvalue  $\nu_0$  is simple, and the corresponding eigenfunction is radially symmetric with constant sign.*

This result was proved in Theorem 2.12 of [14] (see also Lemma 4.2 of [19] and Lemma 1.2 of [24]). When  $\tau = 0$ , the following result on the spectrum of (2.3) was proved in [24]:

**Theorem 2.2** (From [24]): *Let  $\tau = 0$  in (2.3). Assume that either  $m = 2$  and  $1 < p \leq 1 + 4/N$ , or  $m = p + 1$  and  $1 < p < p_c$ , where  $p_c$  is the critical Sobolev exponent in dimension  $N$ . Let  $\lambda \neq 0$  be an eigenvalue of (2.3). Then,  $\text{Re}(\lambda) < 0$ .*

Thus, under the conditions of Theorem 2.2, there are no eigenvalues of (2.3) with positive real parts. However, for any finite value of  $\tau$ , there are always  $N$  zero eigenvalues of (2.3) with corresponding eigenfunctions  $\phi_j = \partial_{y_j} w(|y|)$ , for  $j = 1, \dots, N$ . These are the translation modes. With respect to these eigenfunctions, the nonlocal term in (2.3) vanishes identically. Thus, the translation modes of the local and nonlocal eigenvalue problems coincide. When  $\tau = 0$ , a more refined eigenvalue analysis (cf. [11], [24]) has shown that the presence of the finite domain leads to a slightly different eigenvalue problem than (2.3). This modified eigenvalue problem has the result of perturbing the  $N$  zero eigenvalues of (2.3) so that they become positive, but exponentially small as  $\varepsilon \rightarrow 0$ . Consequently, under the conditions on  $m$  and  $p$  in Theorem 2.2, a one-spike equilibrium solution to (1.3) is unstable, but has an exponentially small growth rate as  $\varepsilon \rightarrow 0$ . This phenomena is called metastability.

In the analysis below, we are not interested in exponentially weak instabilities as  $\varepsilon \rightarrow 0$ . We restrict the analysis to determining any  $O(1)$  instabilities that result from any eigenvalues of (2.3) that cross into the right half-plane  $\text{Re}(\lambda) > 0$  as  $\tau$  is increased. Since  $w$  is radially symmetric, and because the nonlocal term in (2.3) vanishes identically for the nonradially symmetric eigenfunctions of the local operator  $L_0$ , we need only determine the radially symmetric eigenpairs of (2.3) for which the nonlocal term does not vanish.

We now prove the following theorem regarding the spectrum of (2.3) for a special case of the parameters.

**Theorem 2.3:** *Assume that  $m = 2$  and  $1 < p \leq 1 + 4/N$  in (2.3). Then, there exists a unique  $\tau = \tau_0 > 0$  such that the eigenvalue problem (2.3) has an eigenvalue  $\lambda = i\lambda_I^0$ , with  $\lambda_I^0 > 0$ .*

This result suggests that there could be a Hopf bifurcation at  $\tau = \tau_0$ . Lemma 3.1 below, and the numerical computations in §5, establish a clear transversality condition at this bifurcation point. Thus, under the conditions of Theorem 2.3, there is a Hopf bifurcation at  $\tau = \tau_0$ . Numerical values for  $\lambda_I^0$  and  $\tau_0$  are given in §3 for various exponent sets  $(p, q, m, s)$  and dimensions  $N$ .

To prove this theorem we begin by defining the multiplier  $\chi(\tau\lambda)$  by

$$\chi(\tau\lambda) \equiv \frac{2q}{s + 1 + \frac{\tau\lambda}{\mu}}. \quad (2.5)$$

Let  $\psi(y)$  be the solution to

$$L_0\psi = \lambda\psi + w^p; \quad \psi \rightarrow 0 \quad \text{as} \quad |y| \rightarrow \infty. \quad (2.6)$$

Then, the eigenfunctions of (2.3) can be written as

$$\phi = J\chi(\tau\lambda)\psi, \quad J \equiv \frac{\int_{\mathbb{R}^N} w\phi \, dy}{\int_{\mathbb{R}^N} w^2 \, dy}. \quad (2.7)$$

As discussed above, we can assume that  $\int_{\mathbb{R}^N} w\phi \, dy \neq 0$ . Thus, from (2.7), we get

$$\frac{1}{\chi(\tau\lambda)} = \frac{\int_{\mathbb{R}^N} w\psi \, dy}{\int_{\mathbb{R}^N} w^2 \, dy} = \frac{s+1 + \tau\lambda/\mu}{2q}. \quad (2.8)$$

We now look for a pure imaginary eigenvalue of the form  $\lambda = i\lambda_I$ . Without loss of generality we may assume that  $\lambda_I > 0$ .

We first show that  $\lambda_I$  is unique. We write  $\psi$  as  $\psi = \psi_R + i\psi_I$ . Then, decomposing (2.8) in terms of real and imaginary parts, we get

$$\frac{\int_{\mathbb{R}^N} w\psi_R \, dy}{\int_{\mathbb{R}^N} w^2 \, dy} = \frac{(s+1)}{2q}, \quad (2.9 a)$$

$$\frac{\int_{\mathbb{R}^N} w\psi_I \, dy}{\int_{\mathbb{R}^N} w^2 \, dy} = \frac{\tau\lambda_I}{2q\mu}. \quad (2.9 b)$$

Notice that (2.9 a) does not involve  $\tau$ .

Next, we calculate  $\int_{\mathbb{R}^N} w\psi_R \, dy$ . Decomposing (2.6) into real and imaginary parts, we obtain

$$L_0\psi_R = -\lambda_I\psi_I + w^p; \quad L_0\psi_I = \lambda_I\psi_R. \quad (2.10)$$

Combining the two equations in (2.10), we get  $(L_0^2 + \lambda_I^2)\psi_I = \lambda_I w^p$ . Hence,

$$\psi_I = \lambda_I [L_0^2 + \lambda_I^2]^{-1} w^p; \quad \psi_R = L_0 [L_0^2 + \lambda_I^2]^{-1} w^p. \quad (2.11)$$

Define the function  $f_R(\lambda_I)$  by

$$f_R(\lambda_I) \equiv \frac{\int_{\mathbb{R}^N} w L_0 [L_0^2 + \lambda_I^2]^{-1} w^p \, dy}{\int_{\mathbb{R}^N} w^2 \, dy}. \quad (2.12)$$

Substituting (2.11) into (2.9), we obtain the two equations

$$f_R(\lambda_I) = \frac{(s+1)}{2q}, \quad (2.13 a)$$

$$\frac{\tau}{2q\mu} = \frac{\int_{\mathbb{R}^N} w [L_0^2 + \lambda_I^2]^{-1} w^p \, dy}{\int_{\mathbb{R}^N} w^2 \, dy}. \quad (2.13 b)$$

We now show that there is a unique root to (2.13 a) on the interval  $0 < \lambda_I < \infty$ . Since  $L_0$  is self-adjoint, we can integrate by parts in (2.12), and use (2.4) for  $L_0 w$ , to get

$$f_R(\lambda_I) = \frac{\int_{\mathbb{R}^N} (L_0 w) [L_0^2 + \lambda_I^2]^{-1} w^p \, dy}{\int_{\mathbb{R}^N} w^2 \, dy} = (p-1) \frac{\int_{\mathbb{R}^N} w^p [L_0^2 + \lambda_I^2]^{-1} w^p \, dy}{\int_{\mathbb{R}^N} w^2 \, dy}. \quad (2.14)$$

Setting  $\lambda_I = 0$  in (2.14), and integrating by parts using (2.4) for  $L_0^{-1}w^p$ , we calculate  $f_R(0)$  as

$$f_R(0) = (p-1) \frac{\int_{\mathbb{R}^N} w^p L_0^{-2} w^p dy}{\int_{\mathbb{R}^N} w^2 dy} = (p-1) \frac{\int_{\mathbb{R}^N} [L_0^{-1} w^p]^2 dy}{\int_{\mathbb{R}^N} w^2 dy} = \frac{1}{(p-1)}. \quad (2.15)$$

Differentiating (2.14) with respect to  $\lambda_I$ , and integrating the resulting expression by parts, we get

$$f'_R(\lambda_I) = -2(p-1)\lambda_I \frac{\int_{\mathbb{R}^N} w^p [L_0^2 + \lambda_I^2]^{-2} w^p dy}{\int_{\mathbb{R}^N} w^2 dy} = -2(p-1)\lambda_I \frac{\int_{\mathbb{R}^N} ([L_0^2 + \lambda_I^2]^{-1} w^p)^2 dy}{\int_{\mathbb{R}^N} w^2 dy} < 0. \quad (2.16)$$

From (2.14),  $f_R(\infty) = 0$ . Thus,  $f_R(\lambda_I)$  is a monotone decreasing function on the interval  $0 < \lambda_I < \infty$ , with  $f_R(0) = 1/(p-1)$ , and  $f_R(\infty) = 0$ . To establish that there is a unique root to (2.13 a), we must show that  $f_R(0) > (s+1)/2q$ . This follows from the inequality (1.2) on the exponents, since when  $m = 2$ , (1.2) implies  $(p-1)^{-1} > (s+1)/(2q)$ . Hence, there is a unique root  $\lambda_I = \lambda_I^0$  to (2.13 a). From (2.13 b), the corresponding unique value of  $\tau$ , labeled by  $\tau_0$ , is

$$\tau_0 = 2q\mu \frac{\int_{\mathbb{R}^N} w [L_0^2 + (\lambda_I^0)^2]^{-1} w^p dy}{\int_{\mathbb{R}^N} w^2 dy}. \quad (2.17)$$

Notice that the proof of this result that  $\lambda_I^0$  is unique required only that  $m = 2$ , with no restrictions on  $p$  and  $N$  other than (1.2).

It remains to prove the more difficult inequality that  $\tau_0 > 0$ . Let  $\phi_0$  denote the eigenfunction of (2.3) with  $\lambda_0 \equiv i\lambda_I^0$  and  $m = 2$ . Then, from (2.3) and (2.5), we have

$$L_0 \phi_0 - \chi(\tau_0 \lambda_0) w^p \left( \frac{\int_{\mathbb{R}^N} w \phi_0 dy}{\int_{\mathbb{R}^N} w^2 dy} \right) = \lambda_0 \phi_0, \quad (2.18 a)$$

$$L_0 \overline{\phi_0} - \overline{\chi(\tau_0 \lambda_0)} w^p \left( \frac{\int_{\mathbb{R}^N} w \overline{\phi_0} dy}{\int_{\mathbb{R}^N} w^2 dy} \right) = \overline{\lambda_0} \overline{\phi_0}. \quad (2.18 b)$$

Multiplying (2.18 a) by  $\overline{\phi_0}$ , and integrating by parts over  $\mathbb{R}^N$ , we get

$$-\chi(\tau_0 \lambda_0) \frac{(\int_{\mathbb{R}^N} w \phi_0 dy)(\int_{\mathbb{R}^N} w^p \overline{\phi_0} dy)}{\int_{\mathbb{R}^N} w^2 dy} - \lambda_0 \int_{\mathbb{R}^N} |\phi_0|^2 dy = \int_{\mathbb{R}^N} (|\nabla \phi_0|^2 + |\phi_0|^2 - p w^{p-1} |\phi_0|^2) dy. \quad (2.19)$$

Here  $|v|^2 = v\overline{v}$ . Next, we multiply (2.18 a) by  $w$ , and integrate by parts over  $\mathbb{R}^N$ . Then, using  $L_0 w = (p-1)w^p$ , we get

$$(p-1) \int_{\mathbb{R}^N} w^p \phi_0 dy - \chi(\tau_0 \lambda_0) \frac{(\int_{\mathbb{R}^N} w \phi_0 dy)(\int_{\mathbb{R}^N} w^{p+1} dy)}{\int_{\mathbb{R}^N} w^2 dy} = \lambda_0 \int_{\mathbb{R}^N} w \phi_0 dy. \quad (2.20)$$

We solve for  $\int_{\mathbb{R}^N} w^p \phi_0 dy$  in (2.20) and take the conjugate of the resulting expression. Then, using the relation  $\overline{\chi(\tau_0 \lambda_0)} = \chi(\tau_0 \overline{\lambda_0})$ , we obtain

$$\int_{\mathbb{R}^N} w^p \overline{\phi_0} dy = \frac{1}{p-1} \left[ \overline{\lambda_0} + \chi(\tau_0 \overline{\lambda_0}) \left( \frac{\int_{\mathbb{R}^N} w^{p+1} dy}{\int_{\mathbb{R}^N} w^2 dy} \right) \right] \int_{\mathbb{R}^N} w \overline{\phi_0} dy. \quad (2.21)$$

Substituting (2.21) into (2.19), we get

$$\begin{aligned} & -\frac{\chi(\tau_0\lambda_0)}{p-1} \left[ \bar{\lambda}_0 + \chi(\tau_0\bar{\lambda}_0) \left( \frac{\int_{\mathbb{R}^N} w^{p+1} dy}{\int_{\mathbb{R}^N} w^2 dy} \right) \right] \frac{|\int_{\mathbb{R}^N} w\phi_0 dy|^2}{\int_{\mathbb{R}^N} w^2 dy} - \lambda_0 \int_{\mathbb{R}^N} |\phi_0|^2 dy \\ & = \int_{\mathbb{R}^N} (|\nabla\phi_0|^2 + |\phi_0|^2 - pw^{p-1}|\phi_0|^2) dy. \end{aligned} \quad (2.22)$$

The real part of (2.22) is

$$\begin{aligned} & \int_{\mathbb{R}^N} (|\nabla\phi_0|^2 + |\phi_0|^2 - pw^{p-1}|\phi_0|^2) dy \\ & = -\operatorname{Re} \left( \frac{\chi(\tau_0\lambda_0)}{p-1} \left[ \bar{\lambda}_0 + \chi(\tau_0\bar{\lambda}_0) \left( \frac{\int_{\mathbb{R}^N} w^{p+1} dy}{\int_{\mathbb{R}^N} w^2 dy} \right) \right] \right) \frac{|\int_{\mathbb{R}^N} w\phi_0 dy|^2}{\int_{\mathbb{R}^N} w^2 dy}. \end{aligned} \quad (2.23)$$

The next step in the proof that  $\tau_0 > 0$  uses the following key lemma proved in [24]:

**Lemma 2.4** (From [24]): *Assume that  $1 < p \leq 1 + 4/N$ . Let  $v$  be any real function with  $v \in \mathcal{H}^1(\mathbb{R}^N)$ . Then,*

$$\begin{aligned} & \int_{\mathbb{R}^N} (\nabla v \cdot \nabla v + v^2 - pw^{p-1}v^2) dy \geq -2(p-1) \frac{(\int_{\mathbb{R}^N} wv dy) (\int_{\mathbb{R}^N} w^p v dy)}{\int_{\mathbb{R}^N} w^2 dy} \\ & \quad + (p-1) \frac{\int_{\mathbb{R}^N} w^{p+1} dy}{(\int_{\mathbb{R}^N} w^2 dy)^2} \left( \int_{\mathbb{R}^N} wv dy \right)^2. \end{aligned} \quad (2.24)$$

This is Lemma 5.1 of [24]. For completeness, we give the proof below in Appendix A.

This lemma is used to get a lower bound on the left-hand side of (2.23). Decompose  $\phi_0$  as  $\phi_0 = \phi_{0R} + i\phi_{0I}$ . By substituting  $v = \phi_{0R}$  and  $v = \phi_{0I}$  into (2.24), we can then simply add the resulting two inequalities to get

$$\begin{aligned} & \int_{\mathbb{R}^N} (|\nabla\phi_0|^2 + |\phi_0|^2 - pw^{p-1}|\phi_0|^2) dy \geq -\frac{2(p-1)}{(\int_{\mathbb{R}^N} w^2 dy)} \operatorname{Re} \left[ \left( \int_{\mathbb{R}^N} w\phi_0 dy \right) \left( \int_{\mathbb{R}^N} w^p \bar{\phi}_0 dy \right) \right] \\ & \quad + (p-1) \frac{(\int_{\mathbb{R}^N} w^{p+1} dy) |\int_{\mathbb{R}^N} w\phi_0 dy|^2}{(\int_{\mathbb{R}^N} w^2 dy)^2}. \end{aligned} \quad (2.25)$$

Substituting (2.21) into (2.25), we get

$$\begin{aligned} & \int_{\mathbb{R}^N} (|\nabla\phi_0|^2 + |\phi_0|^2 - pw^{p-1}|\phi_0|^2) dy \geq (p-1) \frac{(\int_{\mathbb{R}^N} w^{p+1} dy)}{(\int_{\mathbb{R}^N} w^2 dy)^2} \left| \int_{\mathbb{R}^N} w\phi_0 dy \right|^2 \\ & \quad - \frac{2}{(\int_{\mathbb{R}^N} w^2 dy)} \operatorname{Re} \left[ \bar{\lambda}_0 + \chi(\tau_0\bar{\lambda}_0) \left( \frac{\int_{\mathbb{R}^N} w^{p+1} dy}{\int_{\mathbb{R}^N} w^2 dy} \right) \right] \left| \int_{\mathbb{R}^N} w\phi_0 dy \right|^2. \end{aligned} \quad (2.26)$$

Combining (2.23) and (2.26), we obtain

$$\begin{aligned} & \operatorname{Re} \left( \frac{\chi(\tau_0\lambda_0)}{p-1} \left[ \bar{\lambda}_0 + \chi(\tau_0\bar{\lambda}_0) \left( \frac{\int_{\mathbb{R}^N} w^{p+1} dy}{\int_{\mathbb{R}^N} w^2 dy} \right) \right] \right) - 2 \operatorname{Re} \left[ \bar{\lambda}_0 + \chi(\tau_0\bar{\lambda}_0) \left( \frac{\int_{\mathbb{R}^N} w^{p+1} dy}{\int_{\mathbb{R}^N} w^2 dy} \right) \right] \\ & \quad + (p-1) \left( \frac{\int_{\mathbb{R}^N} w^{p+1} dy}{\int_{\mathbb{R}^N} w^2 dy} \right) \leq 0. \end{aligned} \quad (2.27)$$

This expression can be simplified to

$$\operatorname{Re} [\bar{\lambda}_0\chi(\tau_0\lambda_0)] + (|\chi(\tau_0\lambda_0)|^2 - 2(p-1)\operatorname{Re} [\chi(\tau_0\bar{\lambda}_0)]) + (p-1)^2 \left( \frac{\int_{\mathbb{R}^N} w^{p+1} dy}{\int_{\mathbb{R}^N} w^2 dy} \right) \leq 0. \quad (2.28)$$

Since  $\chi(\tau_0 \overline{\lambda_0}) = \overline{\chi(\tau_0 \lambda_0)}$ , (2.28) can be written as

$$|\chi(\tau_0 \lambda_0) - (p-1)|^2 \leq -\operatorname{Re} [\overline{\lambda_0} \chi(\tau_0 \lambda_0)] \left( \frac{\int_{\mathbb{R}^N} w^2 dy}{\int_{\mathbb{R}^N} w^{p+1} dy} \right). \quad (2.29)$$

Next, using the definition of  $\chi$  in (2.5) and  $\lambda_0 = i\lambda_I^0$ , we calculate  $\operatorname{Re} [\overline{\lambda_0} \chi(\tau_0 \lambda_0)]$  explicitly. Then, as shown in Appendix B, we can calculate the integral ratio in (2.29) as

$$\frac{\int_{\mathbb{R}^N} w^2 dy}{\int_{\mathbb{R}^N} w^{p+1} dy} = \frac{\int_0^\infty \rho^{N-1} w^2 d\rho}{\int_0^\infty \rho^{N-1} w^{p+1} d\rho} = C_{N,p} \equiv \left[ \frac{N + (p+1)(1-N/2)}{p+1} \right]. \quad (2.30)$$

Finally, substituting these expressions into (2.29), we obtain our key inequality

$$|\chi(\tau_0 \lambda_0) - (p-1)|^2 \leq \left( \frac{2q|\lambda_0|^2 \tau_0 / \mu}{(s+1)^2 + |\lambda_0|^2 \tau_0^2 / \mu^2} \right) C_{N,p}. \quad (2.31)$$

Since  $\chi(0) > (p-1)$  and  $\lambda_0 = i\lambda_I^0$ , the left-hand side of (2.31) is clearly positive. Therefore, we have  $\tau_0 > 0$ . This completes the proof of Theorem 2.3.

As a remark, the proof that  $\tau_0 > 0$  did not rely on any explicit formula for the value of  $\lambda_I^0$ . Since  $0 < f_R(\lambda_I) \leq 1/(p-1) > 0$ , we can obtain any value for  $\lambda_I^0$  in  $(0, \infty)$ , by choosing different values of the ratio  $(s+1)/(2q)$  in (2.9 a). Thus, when  $m = 2$ , we have an indirect proof that

$$\frac{\int_{\mathbb{R}^N} w \psi_I dy}{\int_{\mathbb{R}^N} w^2 dy} = \lambda_I \frac{\int_{\mathbb{R}^N} w [L_0^2 + (\lambda_I)^2]^{-1} w^p dy}{\int_{\mathbb{R}^N} w^2 dy} > 0, \quad \text{for any } \lambda_I > 0. \quad (2.32)$$

The inequality (2.31) gives a bound on  $\tau_0$  and  $\lambda_0$ . From this inequality we now obtain an explicit lower bound on  $\lambda_I^0$ . Substituting (2.5) for  $\chi$  into (2.31), we calculate that

$$\frac{\tau_0^2}{\mu^2} (\lambda_I^0)^2 - \frac{2q\tau_0}{\mu(p-1)^2} (\lambda_I^0)^2 C_{N,p} + \zeta^2 \leq 0, \quad \zeta \equiv \frac{2q}{p-1} - (s+1) > 0. \quad (2.33)$$

Let  $h(\tau_0)$  denote the left-hand side of (2.33). Clearly,  $h(0) > 0$ , and  $h(\tau_0) \rightarrow +\infty$  as  $\tau_0 \rightarrow \infty$ . Thus, we require that  $\lambda_I^0$  be sufficiently large to ensure that  $h(\tau_0)$  has two positive roots  $\tau_\pm$ , with  $h(\tau_0) < 0$  in  $\tau_- < \tau_0/\mu < \tau_+$ . Solving the quadratic inequality in (2.33), we obtain the following more explicit bound:

**Lemma 2.5:** *Assume that  $m = 2$  and  $1 < p \leq 1 + 4/N$ . Let  $\zeta$  and  $C_{N,p}$  be as defined in (2.33) and (2.30), respectively. Then, the critical values  $\tau_0$  and  $\lambda_I^0 > 0$  satisfy,*

$$\lambda_I^0 \geq \frac{\zeta(p-1)^2}{qC_{N,p}}, \quad \tau_- < \frac{\tau_0}{\mu} < \tau_+, \quad (2.34 a)$$

where

$$\tau_\pm \equiv \frac{qC_{N,p}}{(p-1)^2} \pm \sqrt{\left( \frac{qC_{N,p}}{(p-1)^2} \right)^2 - \frac{\zeta^2}{(\lambda_I^0)^2}}. \quad (2.34 b)$$

Another bound on these critical values is readily obtained from (2.18). Multiplying (2.18 a) by  $\overline{\phi_0}$  and (2.18 b) by  $\phi_0$ , we subtract the resulting two equations to get

$$\lambda_I^0 \int_{\mathbb{R}^N} |\phi_0|^2 dy = \operatorname{Im} \left[ \frac{1}{\chi(\tau_0 \lambda_0)} \frac{(\int_{\mathbb{R}^N} w \overline{\phi_0} dy) (\int_{\mathbb{R}^N} w^p \phi_0 dy)}{\int_{\mathbb{R}^N} w^2 dy} \right] \leq \frac{|\chi(\tau_0 \lambda_0)|}{\int_{\mathbb{R}^N} w^2 dy} \left| \int_{\mathbb{R}^N} w \overline{\phi_0} dy \right| \left| \int_{\mathbb{R}^N} w^p \phi_0 dy \right|. \quad (2.35)$$

Using the Cauchy-Schwartz inequality, and a simple bound on  $|\chi|$ , we get

$$\lambda_I^0 \leq |\chi(\tau_0 \lambda_0)| \left( \frac{\int_{\mathbb{R}^N} w^{2p} dy}{\int_{\mathbb{R}^N} w^2 dy} \right)^{1/2} \leq \frac{2q}{(s+1)} \left( \frac{\int_{\mathbb{R}^N} w^{2p} dy}{\int_{\mathbb{R}^N} w^2 dy} \right)^{1/2}. \quad (2.36)$$

The bounds in (2.34) and (2.36) will be evaluated in the next section after we compute the values  $\tau_0$  and  $\lambda_I^0$  numerically.

### 3 Numerical Computations of the Spectrum

In this section we give some numerical results for the spectrum of (2.3) as  $\tau$  is varied. Since the stability results depend only the ratio  $\tau/\mu$ , we will set  $\mu = 1$  in the remainder of the paper.

We first formulate the problem for the eigenvalues of (2.3) and introduce some notation. Let  $g(\lambda)$  be defined by

$$g(\lambda) = \frac{s+1+\tau\lambda}{qm} - f(\lambda), \quad f(\lambda) \equiv \frac{\int_{\mathbb{R}^N} w^{m-1} \psi dy}{\int_{\mathbb{R}^N} w^m dy}, \quad (3.1)$$

where  $\psi$  satisfies (2.6). By repeating the analysis of (2.6)–(2.8), this time for any  $m > 1$ , it follows that the nonzero eigenvalues of (2.3) and the roots of  $g(\lambda) = 0$  coincide exactly. We separate (3.1) into real and imaginary parts by writing

$$g = g_R + i g_I, \quad f = f_R + i f_I, \quad \lambda = \lambda_R + i \lambda_I, \quad \psi = \psi_R + i \psi_I. \quad (3.2)$$

This gives

$$g_R(\lambda) = \frac{s+1+\tau\lambda_R}{qm} - f_R(\lambda), \quad f_R(\lambda) \equiv \frac{\int_{\mathbb{R}^N} w^{m-1} \psi_R dy}{\int_{\mathbb{R}^N} w^m dy}, \quad (3.3 a)$$

$$g_I(\lambda) = \frac{\tau\lambda_I}{qm} - f_I(\lambda), \quad f_I(\lambda) \equiv \frac{\int_{\mathbb{R}^N} w^{m-1} \psi_I dy}{\int_{\mathbb{R}^N} w^m dy}. \quad (3.3 b)$$

From (2.6), the functions  $\psi_R$  and  $\psi_I$  are radially symmetric solutions to

$$L_0 \psi_R = \lambda_R \psi_R - \lambda_I \psi_I + w^p; \quad L_0 \psi_I = \lambda_R \psi_I + \lambda_I \psi_R, \quad (3.4)$$

with  $\psi_R \rightarrow 0$  and  $\psi_I \rightarrow 0$  as  $|y| \rightarrow \infty$ .

In the computations below, we determine the number of zeroes of  $g(\lambda)$  in the right half-plane by calculating the winding number of  $g$  over the counterclockwise contour composed of the imaginary axis  $-iR \leq \text{Im}\lambda \leq iR$  and the semi-circle  $\Gamma_R$ , given by  $|\lambda| = R > 0$ , for  $-\pi/2 \leq \arg\lambda \leq \pi/2$ . Assuming that  $\tau$  is chosen so that there are no zeroes of  $g(\lambda)$  on the imaginary axis, we let  $R \rightarrow \infty$  and use the argument principle to determine the number of zeroes of  $g(\lambda)$  in the right half-plane. A related approach to determine the stability of a spike for the Gray-Scott model in one spatial dimension was used in [7]. In [7], the winding number was used in a rather different manner, namely to count the number of eigenvalues in the neighbourhood of the origin. We use it here to determine the number of eigenvalues in the right-half plane for  $\tau > \tau_0$ .

The function  $g(\lambda)$  in (3.1) is analytic in the right half-plane, except at the simple pole  $\lambda = \nu_0 > 0$ , where

$(p, q, m, s)$	$N$	$\tau_0$	$\lambda_I^0$	(2.34 a) (lower)	(2.36) (upper)
(2, 1, 2, 0)	1	0.771	1.238	1.200	2.484
(2, 1, 2, 0)	2	0.561	1.593	1.500	3.230
(2, 1, 2, 0)	3	0.373	2.174	2.000	4.519
(3, 2, 2, 0)	1	0.304	2.859	2.667	5.842
(3, 2, 2, 0)	2	0.150	4.477	4.000	9.849
(4, 2, 2, 0)	1	0.149	2.525	2.143	6.628

Table 1. Numerical values for  $\tau_0$  and  $\lambda_I^0$  for different exponent sets  $(p, q, m, s)$  and dimension  $N$ . The last two columns are the lower and upper bounds on  $\lambda_I^0$  predicted by (2.34 a) and (2.36), respectively.

$\nu_0$  is the unique positive eigenvalue of the local operator  $L_0$  (see Theorem 2.1 above). For any  $\tau > 0$ , it is clear from (3.1), that since  $|f(\lambda)| = o(1)$  on  $\Gamma_R$  as  $R \rightarrow \infty$ , the change in the argument of  $g$  over  $\Gamma_R$  as  $R \rightarrow \infty$  is simply  $\pi$ . Thus, using  $g(\bar{\lambda}) = \overline{g(\lambda)}$ , and assuming that there are no zeroes of  $g(\lambda)$  on the imaginary axis, the argument principle gives the following formula for the number  $M$  of eigenvalues of (2.3) in the right half-plane  $\text{Re}(\lambda) > 0$ :

$$M = \frac{3}{2} + \frac{1}{\pi} \Delta_{\Gamma_I} g, \quad \text{where } \Delta_{\Gamma_I} g \equiv [\arg g]_{\Gamma_I}, \quad \tau > 0. \quad (3.5)$$

Here  $[\arg g]_{\Gamma_I}$  denotes the change in the argument of  $g$  along the semi-infinite imaginary axis  $\Gamma_I = i\lambda_I$ ,  $0 \leq \lambda_I < \infty$ , traversed in the downwards direction.

In the numerical computations below, we will only consider exponent sets  $(p, q, m, s)$  that were typically chosen in previous modeling of the GM model (cf. [8], [10], [15], [16]). We always assume that the exponent set satisfies (1.2). We further categorize the exponent set and dimension  $N$  as being of Type 1 if they also satisfy the conditions of Theorem 2.3. Data is referred to as being of Type 2 if it satisfies (1.2) and either  $m \neq 2$  or  $p > 1 + 4/N$ . Type 1 data is considered below, and Type 2 data is examined in §4.

### 3.1 Type 1 Data: $m = 2$ , $1 < p \leq 1 + 4/N$

We first use the boundary value problem solver COLSYS [1] to compute the ground state solution  $w$  satisfying (2.2) and the principal eigenpair  $\phi_{l0}$  and  $\nu_0$  of the local operator  $L_0$ , defined in (2.3 c).

To determine the critical values of the parameters for which (2.3) has eigenvalues on the imaginary axis, we set  $\lambda_R = 0$  in (3.1)–(3.4) and compute the point  $\tau = \tau_0$  and  $\lambda = i\lambda_I^0 > 0$  for which  $g(\lambda) = 0$  has a root. To do so, the system (3.4) for  $\psi_R$  and  $\psi_I$  is solved using COLSYS and Euler continuation in the parameter  $\lambda_I$ , starting from the initial point  $\lambda_I = 0$ , where an initial solution  $\psi_R = \frac{w}{p-1}$  and  $\psi_I = 0$  is known. Theorem 2.3 guarantees that  $g_R = 0$  has a unique root  $\lambda_I^0$ , independent of  $\tau$ . This root is first bracketed using a bisection technique, and then solved for accurately using Newton's method. Substituting this value of  $\lambda_I$  into  $g_I = 0$  of (3.3 b), we obtain the unique value  $\tau_0$ . By Theorem 2.3,  $\tau_0 > 0$ .

In Table 1 we give some numerical results for  $\tau_0$  and  $\lambda_I^0$ , accurate to three significant digits, for different exponent sets  $(p, q, m, s)$  and dimension  $N$ . The lower and upper bounds on  $\lambda_I^0$  predicted in (2.34 a) and

(2.36), respectively, are given in the last two columns of this table. From this table we note that the lower bound (2.34 a) for  $\lambda_I^0$  is actually quite close to the numerically computed value. For the exponent set  $(2, 1, 2, 0)$  we use the value of  $\lambda_I^0$  in Table 1, to calculate the bounds (2.34 b) on  $\tau_0$ . We obtain,

$$0.63 \leq \tau_0 \leq 1.04, \quad (N = 1); \quad 0.44 \leq \tau_0 \leq 0.89, \quad (N = 2); \quad 0.24 \leq \tau_0 \leq 0.51, \quad (N = 3). \quad (3.6)$$

These bounds are reasonably narrow, but have the deficiency that they require knowledge of  $\lambda_I^0$ . For this exponent set and for  $N = 1, 2, 3$ , in Fig. 2(a) and Fig. 2(b) we plot the real and imaginary parts of  $\psi$  at the critical point  $\tau_0$  and  $\lambda_I^0$ .

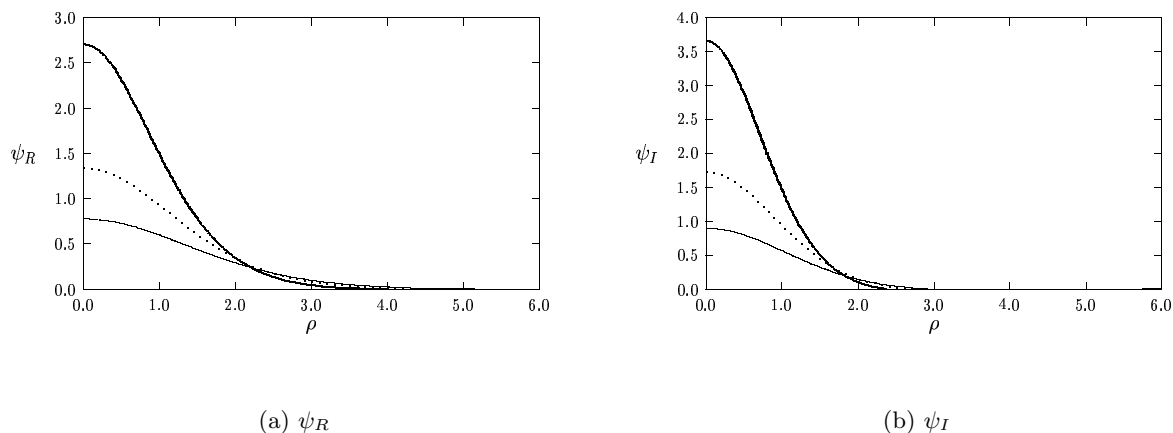


FIGURE 2. Plots of  $\psi_R$  and  $\psi_I$  at  $\lambda_I = \lambda_I^0$  and  $\tau = \tau_0$ , for the exponent set  $(p, q, m, s) = (2, 1, 2, 0)$ . The solid curves are for  $N = 1$ , the dashed curves are for  $N = 2$ , and the heavy solid curves are for  $N = 3$ .

Before computing the number of zeroes in the right half-plane using (3.5), it is convenient to display some of our computational results graphically. For the exponent set  $(p, q, m, s) = (2, 1, 2, 0)$  with  $N = 3$ , in Fig. 3(a) we plot the graphical construction of the determination of a unique root to  $g_R = 0$ . In this figure we plot  $f_R$  as a function of  $\lambda_I$ , and we show the constant value  $(s + 1)/(2q)$ . In the proof of Theorem 2.3, it was shown that  $f_R(0) = 1/(p - 1) > (s + 1)/(2q)$ ,  $f_R$  tends to zero as  $\lambda_I \rightarrow \infty$ , and  $f_R$  is monotonically decreasing for  $\lambda_I > 0$  (see (2.16)). Thus, there is a unique intersection point at some value  $\lambda_I^0$ . At this point  $g_R = 0$ . In Fig. 3(b) we plot the graphical construction of the root of  $g_I = 0$ . In this figure we plot  $f_I$  as a function of  $\lambda_I$  together with the straight line  $\tau_0 \lambda_I / (2q)$ . The value  $\tau = \tau_0$  is chosen so that this line and the curve  $f_I$  intersect at  $\lambda_I^0$ . In the proof of Theorem 2.3, we concluded that  $f_I > 0$  for  $\lambda_I > 0$ , with  $f_I(0) = 0$  and  $f_I \rightarrow 0$  as  $\lambda_I \rightarrow \infty$ . However, we do not have a proof that for any Type 1 data  $f_I$  has a unique maximum point such as that shown numerically in Fig. 3(b) for the exponent set  $(p, q, m, s) = (2, 1, 2, 0)$  with  $N = 3$ . Fortunately, we do not need a detailed knowledge of the behaviour of  $f_I$  in order to calculate the number of zeroes in the right half-plane using (3.5).

We now determine the number of eigenvalues of (2.3) in the right half-plane as  $\tau$  is varied. Let  $\Delta_{\Gamma_i} g$  be

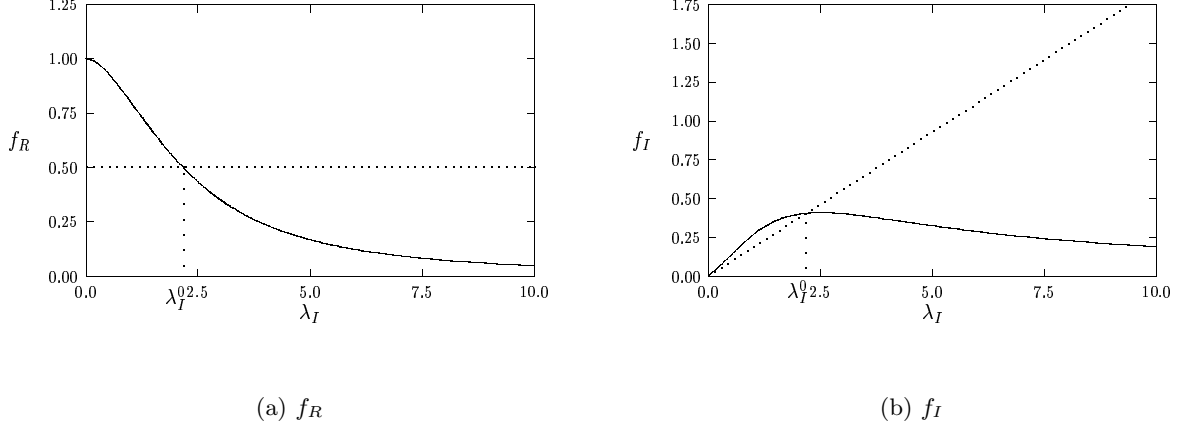


FIGURE 3. Plots of  $f_R$  and  $f_I$  versus  $\lambda_I$  for the exponent set  $(p, q, m, s) = (2, 1, 2, 0)$  with  $N = 3$ . The horizontal dashed line in the leftmost figure is the value  $(s + 1)/(2q)$ , which intersects  $f_R$  at  $\lambda_I^0 = 2.174$ . At this point  $g_R = 0$ . The critical value  $\tau = \tau_0 = 0.373$  is chosen so that the dashed line in the rightmost figure with slope  $\tau/(2q)$  intersects  $f_I$  at  $\lambda = \lambda_I^0$ . At this point,  $g_I = 0$ .

the change in the argument of  $g$  along the semi-infinite imaginary axis  $\lambda_I \geq 0$  traversed in the downwards direction. It is easy to calculate  $\Delta_{\Gamma_i} g$  as  $\tau$  is varied, and then determine the number  $M$  of eigenvalues of (2.3) in the right half-plane using (3.5). We obtain the following result:

**Lemma 3.1:** *Assume that  $m = 2$  and  $1 < p \leq 1 + 4/N$ . Then, for all  $\tau > \tau_0$  there are exactly two eigenvalues of (2.3) in the right half-plane  $\text{Re}(\lambda) > 0$ . Alternatively, for all  $\tau$  with  $0 < \tau < \tau_0$  there are no eigenvalues of (2.3) in the right half-plane.*

The proof of this result is easy using the formulae for  $g_R$  and  $g_I$  with  $\lambda_R = 0$  in (3.3). From the proof of Theorem 2.3,  $g_R = 0$  has a unique simple root at  $\lambda_I^0 > 0$ , with  $g_R > 0$  on  $\lambda_I > \lambda_I^0$  and  $g_R < 0$  on  $0 \leq \lambda_I < \lambda_I^0$ . Note that  $g_R$  is bounded as  $\lambda_I \rightarrow \infty$ . For any  $\tau > 0$ ,  $g_I \rightarrow +\infty$  as  $\lambda_I \rightarrow \infty$ . Hence, the starting point for the argument is  $\tan^{-1}(g_I/g_R) \rightarrow \pi/2$  as  $\lambda_I \rightarrow +\infty$ . At  $\lambda_I = 0$ , we have  $g_R < 0$  and  $g_I = 0$ . Thus, the ending point for the argument is on the negative real axis in the  $g_I, g_R$  plane. Since  $g_R = 0$  only at  $\lambda_I^0$ , we must determine the sign of  $g_I$  at this point. Using (3.3 b) with  $\lambda_R = 0$ , we calculate  $g_I = (\tau - \tau_0)\lambda_I^0$  at  $\lambda_I = \lambda_I^0$ . Hence, for any  $\tau$  with  $0 < \tau < \tau_0$ , the crossing of the imaginary axis occurs in  $g_I < 0$ . This implies that  $\Delta_{\Gamma_i} g = -3\pi/2$ , and from (3.5) we get  $M = 0$ . Alternatively, for any  $\tau > \tau_0$ ,  $g_I > 0$  when  $g_R = 0$ . Thus,  $\Delta_{\Gamma_i} g = \pi/2$ , and from (3.5) we get  $M = 2$ . Since there are exactly two eigenvalues with  $\text{Re}(\lambda) > 0$  when  $\tau > \tau_0$ , either they are both real and positive, or else they are complex conjugates with positive real parts. This completes the proof of Lemma 3.1.

The formula  $g_I = (\tau - \tau_0)\lambda_I^0$  at  $\lambda_I = \lambda_I^0$  where  $g_R = 0$  also shows a strict transversality condition as  $\tau$  crosses through  $\tau_0$ . Thus, we can conclude that there is indeed a Hopf bifurcation at  $\tau = \tau_0$  and  $\lambda_I = \lambda_I^0$ .

Next, we track the roots of  $g(\lambda) = 0$  as they enter the right half-plane. To do so, we solve the system (3.4) using COLSYS, and then determine the zeroes of  $g(\lambda)$  in (3.1) using Newton's method at each  $\tau > \tau_0$ . Using

Euler continuation, we then determine the path  $\lambda(\tau) = \lambda_R(\tau) + i\lambda_I(\tau)$  as  $\tau$  is increased past  $\tau_0$ . We also followed this path into the left half-plane as  $\tau$  is decreased below  $\tau_0$ . Eventually as  $\tau < \tau_0$  became sufficiently small, our Newton iteration scheme failed to converge. We speculate that this is a result of a complicated branching structure of the eigenvalues in the left half-plane when  $\tau$  is small originating from the continuous spectrum along the segment  $\lambda_I = 0$  and  $\lambda_R < -1$ .

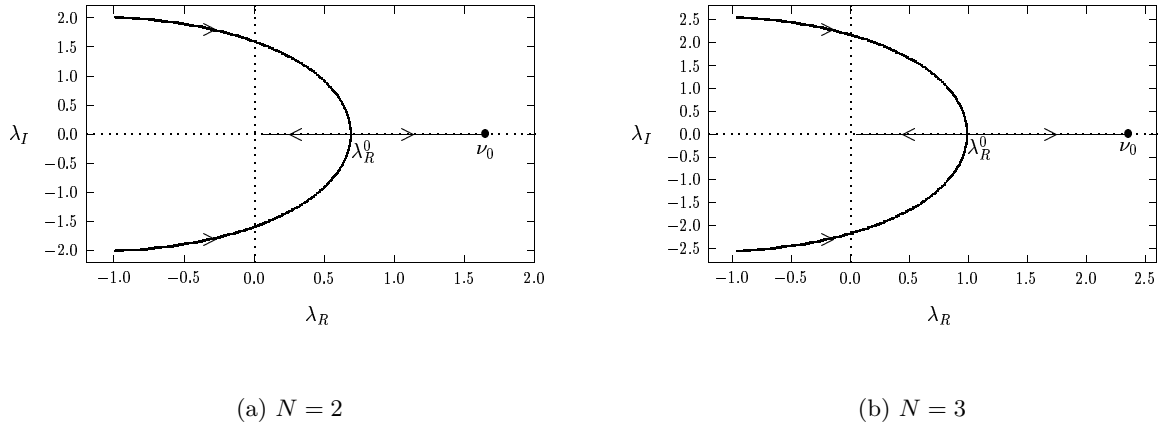


FIGURE 4. Plots of the path of  $\lambda = \lambda_R + i\lambda_I$ , and its conjugate, for  $(p, q, m, s) = (2, 1, 2, 0)$  with  $N = 2$  and  $N = 3$ . The arrows indicate the direction of increasing  $\tau$ . The complex conjugate pair merge onto the real axis at  $\lambda_R^0$ . One eigenvalue then tends to the eigenvalue  $\nu_0 > 0$  of  $L_0$  as  $\tau \rightarrow \infty$ .

For the exponent set  $(p, q, m, s) = (2, 1, 2, 0)$ , in Fig. 4(a) and Fig. 4(b) we show this path in the complex plane for  $N = 2$  and  $N = 3$ , respectively. The results show that the complex eigenvalue and its conjugate merge at a point  $\lambda_R^0$  on the positive real axis at some value  $\tau_c$ . Then, for  $\tau > \tau_c$ , the eigenvalues remain along the real axis with the larger eigenvalue tending to  $\nu_0$  as  $\tau \rightarrow \infty$ , and the smaller eigenvalue tending to zero as  $\tau \rightarrow \infty$ . In Fig. 5(a) and Fig. 5(b) we plot the real and imaginary parts of the eigenvalue with positive imaginary part on the interval  $\tau < \tau_c$  for  $N = 2$  and  $N = 3$ , respectively. This type of path in the spectrum is very similar to what was shown for the Gray-Scott model in one spatial dimension in [6] and [7].

To determine the criteria for eigenvalues of (2.3) on the real axis, we set  $\lambda_I = 0$  in (3.1)–(3.4). The eigenvalues on the real axis are the roots of  $g_R(\lambda_R) = 0$ , which gives

$$\frac{s + 1 + \tau\lambda_R}{2q} = f_R(\lambda_R) \equiv \frac{\int_{\mathbb{R}^N} w\psi_R dy}{\int_{\mathbb{R}^N} w^2 dy}. \quad (3.7 a)$$

Setting  $\lambda_I = 0$  in (3.4), we calculate

$$\psi_R = (L_0 - \lambda_R)^{-1} w^p. \quad (3.7 b)$$

Therefore,  $f_R \rightarrow +\infty$  as  $\lambda_R \rightarrow \nu_0^-$ , where  $\nu_0 > 0$  is the principal eigenvalue of  $L_0$ . Thus,  $g_R = 0$  on the

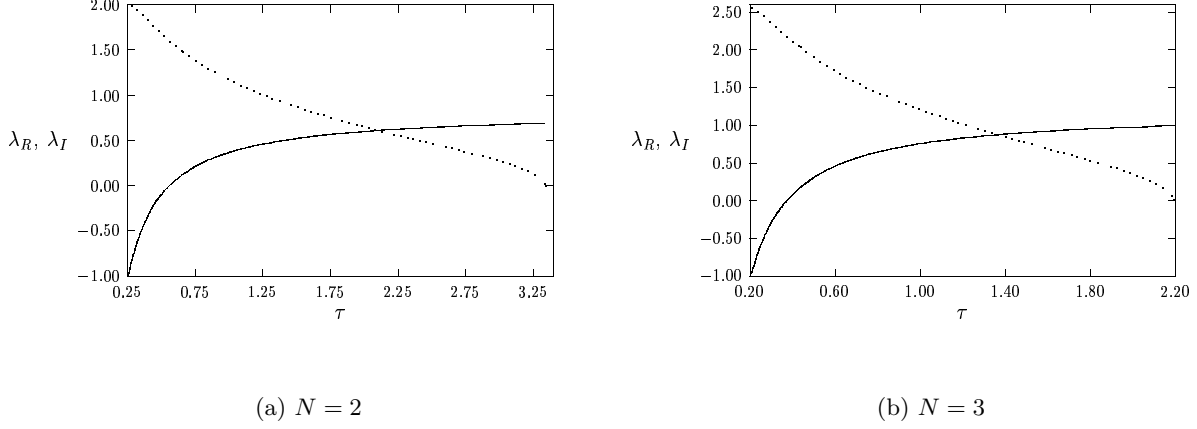


FIGURE 5. Plots of  $\lambda_R$  (solid curve) and  $\lambda_I \geq 0$  (dashed curve) versus  $\tau$  on the interval  $\tau < \tau_c$  for the exponent set  $(p, q, m, s) = (2, 1, 2, 0)$  with  $N = 2$  and  $N = 3$ . Note that  $\lambda_R = 0$  when  $\tau = \tau_0$  and as  $\tau \rightarrow \tau_c$ , we have  $\lambda_I \rightarrow 0$  and  $\lambda_R \rightarrow \lambda_R^0$ .

interval  $0 < \lambda_R < \nu_0$  when

$$\tau = E(\lambda_R), \quad \text{where} \quad E(\lambda_R) \equiv \frac{1}{\lambda_R} [2qf_R(\lambda_R) - (s + 1)]. \quad (3.8)$$

We can use (2.4) and (3.7 b) to calculate that  $f_R(0) = 1/(p - 1)$ . Hence, from condition (1.2) on the exponents,  $E \rightarrow +\infty$  as  $\lambda_R \rightarrow 0$ . Also  $E \rightarrow +\infty$  as  $\lambda_R \rightarrow \nu_0^-$ . The function  $E$  is continuous on  $0 < \lambda_R < \nu_0$ . For the exponent set  $(p, q, m, s) = (2, 1, 2, 0)$ , in Fig. 6(a) and Fig. 6(b) we plot the numerically computed function  $E(\lambda_R)$  on the interval  $0 < \lambda_R < \nu_0$  for  $N = 2$  and  $N = 3$ , respectively. The value of  $\tau$  at which the complex conjugate pair of eigenvalues hit the real axis is obtained from the minimization condition

$$\tau_c = \min_{0 < \lambda_R < \nu_0} E(\lambda_R). \quad (3.9)$$

The inequality  $\tau_c > 0$  follows immediately since  $\tau_c > \tau_0$  and  $\tau_0 > 0$  from Theorem 2.3. Hence,  $E(\lambda_R) > 0$  on  $0 < \lambda_R < \nu_0$ . In addition, since we proved in Lemma 3.1 that there are exactly two eigenvalues in the right half-plane for each  $\tau > \tau_0$ , and since  $E \rightarrow +\infty$  as  $\lambda_R \rightarrow 0$  and as  $\lambda_R \rightarrow \nu_0^-$  it follows that there must be exactly two roots to  $\tau = E(\lambda_R)$  for each  $\tau > \tau_c$ . This implies that for Type 1 data, the function  $E(\lambda_R)$  must have exactly one minimum point at some  $\lambda_R^0$ , and no other local maxima or minima. Thus, once the complex conjugate eigenvalues have merged onto the real axis at  $\lambda_R^0$  when  $\tau = \tau_c$ , they must remain on the real axis for all  $\tau > \tau_c$ .

We use a bisection algorithm to locate the critical values  $\tau = \tau_c$  and  $\lambda = \lambda_R^0$  numerically. The results, accurate to three significant digits, are given in Table 2.

For each  $\tau > \tau_c$ , there are two eigenvalues along the positive real axis. For  $\tau \gg 1$ , there is one eigenvalue with  $\lambda = O(1)$  and another with  $\lambda = O(1/\tau)$ . The eigenvalue with  $\lambda = O(1)$  will tend to  $\nu_0^-$  as  $\tau \rightarrow \infty$ .

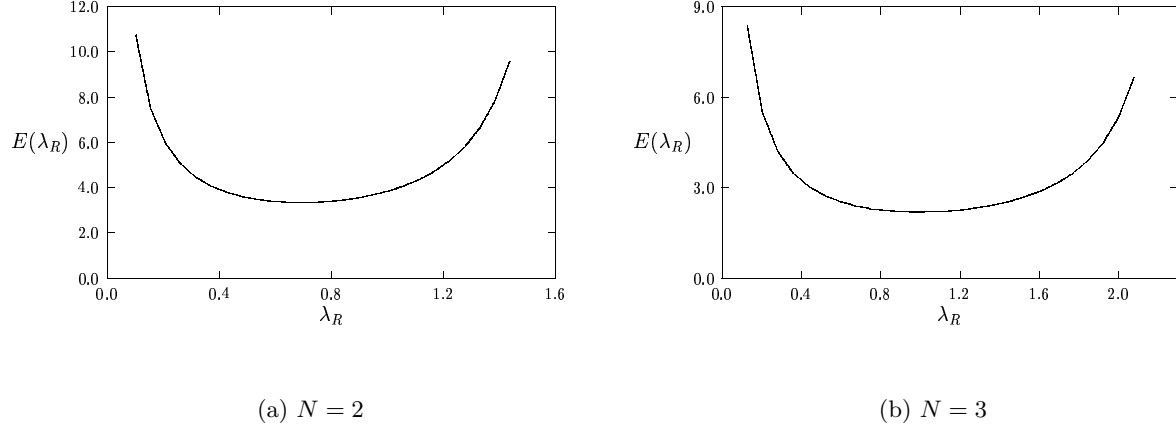


FIGURE 6. Plots of  $E(\lambda_R)$  defined in (3.8) versus  $\lambda_R$  on the interval  $0 < \lambda_R < \nu_0$ , where  $\nu_0 > 0$  is the principal eigenvalue of  $L_0$ . The exponent set is  $(p, q, m, s) = (2, 1, 2, 0)$  and  $N = 2$  (leftmost figure) or  $N = 3$  (rightmost figure). In each case,  $E(\lambda_R)$  has a unique minimum point at some  $\lambda_R^0$ , with minimum value  $\tau_c = E(\lambda_R^0)$ .

$(p, q, m, s)$	$N$	$\tau_c$	$\lambda_R^0$	$\nu_0$
$(2, 1, 2, 0)$	1	4.560	0.526	1.25
$(2, 1, 2, 0)$	2	3.338	0.691	1.65
$(2, 1, 2, 0)$	3	2.189	0.997	2.36
$(3, 2, 2, 0)$	1	1.800	1.263	3.00
$(3, 2, 2, 0)$	2	0.843	2.294	5.41
$(4, 2, 2, 0)$	1	0.471	1.826	5.25

Table 2. Numerical values for  $\tau_c$  and  $\lambda_R^0$  for different exponent sets  $(p, q, m, s)$  and dimension  $N$ . The last column is the principal eigenvalue  $\nu_0$  of the local operator  $L_0$ .

The principal eigenvalue  $\nu_0 > 0$  of the local operator depends only on  $p$  and  $N$ . Numerical values for  $\nu_0$ , computed to two significant digits, are given in the last column of Table 2.

We now derive asymptotic formulae for the eigenvalues and their corresponding eigenfunctions in the limit  $\tau \rightarrow \infty$ . Since the validity of these formulae does not depend on  $m$ , we will for the moment consider any  $m > 1$ .

The eigenvalue  $\lambda_s$  tending to zero as  $\tau \rightarrow \infty$ , and its corresponding eigenfunction  $\psi_s$ , are expanded as

$$\lambda_R = \lambda_s \sim \frac{\beta_0}{\tau} + \frac{\beta_1}{\tau^2} + \dots; \quad \psi_R = \psi_s \sim \psi_{s0} + \frac{\psi_{s1}}{\tau} + \dots. \quad (3.10)$$

Substituting this expansion into (3.4) with  $\lambda_I = 0$ , we collect powers of  $1/\tau$  to get

$$L_0 \psi_{s0} = w^p, \quad \frac{s+1+\beta_0}{qm} = \frac{\int_{\mathbb{R}^N} w^{m-1} \psi_{s0} dy}{\int_{\mathbb{R}^N} w^m dy}, \quad (3.11 a)$$

$$L_0 \psi_{s1} = \beta_0 \psi_{s0}, \quad \frac{\beta_1}{qm} = \frac{\int_{\mathbb{R}^N} w^{m-1} \psi_{s1} dy}{\int_{\mathbb{R}^N} w^m dy}. \quad (3.11 b)$$

Using (2.4) for  $L_0^{-1}w$  and  $L_0^{-1}w^p$ , we readily calculate that

$$\psi_{s0} = \frac{w}{p-1}, \quad \psi_{s1} = \frac{\beta_0}{p-1} \left( \frac{w}{p-1} + \frac{1}{2}\rho w' \right). \quad (3.12)$$

An equation for  $\beta_0$  is obtained by substituting  $\psi_{s0}$  into the integral in (3.11 a). Solving this equation, we get

$$\beta_0 = \zeta, \quad (3.13)$$

where  $\zeta$  is defined in (1.2). Finally, substituting  $\psi_{s1}$  given in (3.12) into the integral in (3.11 b), and integrating the resulting expression by parts, we get

$$\beta_1 = \frac{qm\zeta}{p-1} \left[ \frac{1}{p-1} + \frac{1}{2m} \left( \frac{\int_0^\infty \rho^N (w^m)' d\rho}{\int_0^\infty \rho^{N-1} w^m d\rho} \right) \right] = \frac{qm\zeta}{p-1} \left[ \frac{1}{p-1} - \frac{N}{2m} \right]. \quad (3.14)$$

Therefore, a two-term expansion for the eigenvalue on the real axis with  $\lambda_R = O(1/\tau)$  as  $\tau \rightarrow \infty$  is

$$\lambda_s \sim \frac{\zeta}{\tau} + \frac{qm\zeta}{\tau^2(p-1)} \left[ \frac{1}{p-1} - \frac{N}{2m} \right] + \dots, \quad (3.15 a)$$

$$\psi_s \sim \frac{w}{p-1} + \frac{\zeta}{\tau(p-1)} \left( \frac{w}{p-1} + \frac{1}{2}\rho w' \right) + \dots, \quad (3.15 b)$$

where  $\zeta$  is given in (3.13).

Next, we consider the eigenvalue  $\lambda_R$  with  $\lambda_R = O(1)$  as  $\tau \rightarrow \infty$ . Since this implies that  $g_R(\lambda_R)$  is unbounded as  $\tau \rightarrow \infty$ , this eigenvalue must be close to the eigenvalue  $\nu_0 > 0$  of the local operator  $L_0$ . This eigenpair, denoted by  $\lambda_b$  and  $\psi_b$ , is expanded as

$$\lambda_R = \lambda_b \sim \delta_0 + \frac{\delta_1}{\tau} + \dots; \quad \psi_R = \psi_b \sim \tau\psi_{b0} + \psi_{b1} + \dots. \quad (3.16)$$

Substituting (3.16) into (3.4) with  $\lambda_I = 0$ , and collecting powers of  $1/\tau$ , we obtain

$$L_0\psi_{b0} - \delta_0\psi_{b0} = 0; \quad L_0\psi_{b1} - \delta_0\psi_{b1} = \delta_1\psi_{b0} + w^p. \quad (3.17)$$

Thus,  $\delta_0 = \nu_0 > 0$  and  $\psi_{b0} = A_0\phi_{l0}$ , where  $A_0$  is an unknown constant. Here  $\phi_{l0}$  is the principal eigenfunction of the local operator  $L_0$  (see Theorem 2.1). We may assume that  $\phi_{l0}$  is normalized so that  $\int_{\mathbb{R}^N} \phi_{l0}^2 dy = 1$ . Then, the solvability condition for the equation for  $\psi_{b1}$  in (3.17) determines  $\delta_1$  as

$$\delta_1 = -A_0^{-1} \int_{\mathbb{R}^N} w^p \phi_{l0} dy. \quad (3.18)$$

To determine  $A_0$ , we substitute (3.16) into (3.3 a) to locate a root of  $g_R = 0$ . Collecting the  $O(\tau)$  terms, and then substituting  $\delta_0 = \nu_0$  and  $\psi_{b0} = A_0\phi_{l0}$  into the resulting expression, we obtain an equation for  $A_0$ . Solving this equation, we get

$$A_0 = \frac{\nu_0}{qm} \left( \frac{\int_{\mathbb{R}^N} w^m dy}{\int_{\mathbb{R}^N} w^{m-1} \phi_{l0} dy} \right). \quad (3.19)$$

In this way, we obtain the following two-term expansion for the eigenpair with  $\lambda_R = O(1)$  as  $\tau \rightarrow \infty$ :

$$\lambda_b \sim \nu_0 - \frac{1}{A_0\tau} \int_{\mathbb{R}^N} w^p \phi_{l0} dy + \dots; \quad \psi_b \sim \tau A_0\phi_{l0} + \psi_{b1} + \dots. \quad (3.20)$$

Here  $A_0$  is defined in (3.19).

For the exponent set  $(p, q, m, s) = (2, 1, 2, 0)$  with  $N = 2$ , in Fig. 7(a) and Fig. 7(b) we compare the numerical values for  $\lambda_b$  and  $\lambda_s$  with the corresponding asymptotic results (3.20) and (3.15). These figures show a clear agreement between the asymptotic and numerical results even for only moderately large values of  $\tau$ .

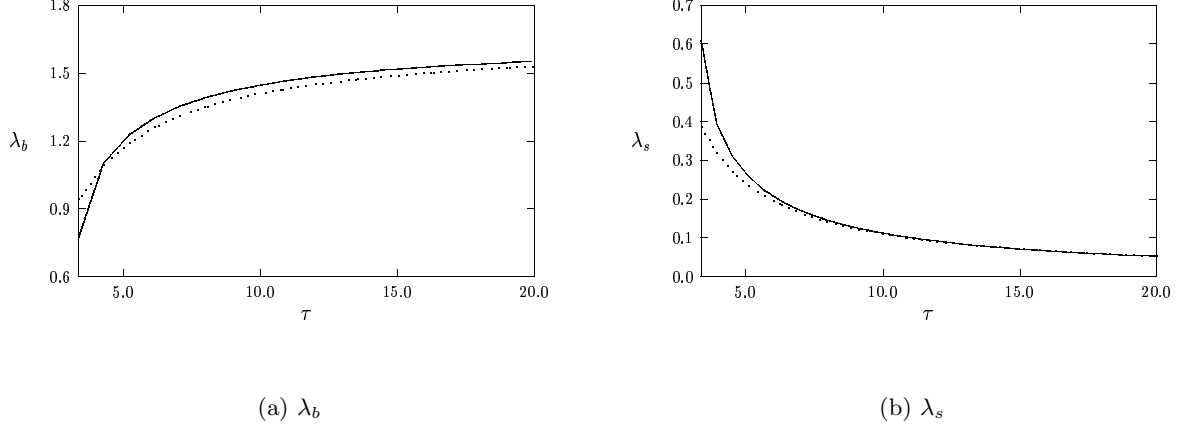


FIGURE 7. Plot of the large eigenvalue  $\lambda_R = \lambda_b$  (leftmost figure) and the small eigenvalue  $\lambda_R = \lambda_s$  (rightmost figure) that are along the real axis for  $\tau > \tau_c$ . The dashed lines are the asymptotic approximations for  $\lambda_b$  and  $\lambda_s$  for large  $\tau$  given in (3.20) and (3.15), respectively. The exponent set is  $(p, q, m, s) = (2, 1, 2, 0)$  with  $N = 2$ .

#### 4 Type 2 Data: $m \neq 2$ or $p > 1 + 4/N$

We begin by looking for a Hopf bifurcation point on the imaginary axis. Setting  $\lambda_R = 0$  in (3.3) and (3.4), the possible bifurcation points are roots of  $g_R = g_I = 0$ , where

$$g_R(\lambda_I) = \frac{s+1}{qm} - f_R(\lambda_I), \quad f_R(\lambda_I) \equiv \frac{\int_{\mathbb{R}^N} w^{m-1} L_0 [L_0^2 + \lambda_I^2]^{-1} w^p dy}{\int_{\mathbb{R}^N} w^m dy}, \quad (4.1 a)$$

$$g_I(\lambda) = \frac{\tau \lambda_I}{qm} - f_I(\lambda), \quad f_I(\lambda_I) \equiv \lambda_I \frac{\int_{\mathbb{R}^N} w^{m-1} [L_0^2 + \lambda_I^2]^{-1} w^p dy}{\int_{\mathbb{R}^N} w^m dy}. \quad (4.1 b)$$

To get some insight into the difference between Type 1 and Type 2 data, we calculate the behaviour of  $f_R$  and  $f_I$  as  $\lambda_I \rightarrow 0$ . For  $\lambda_I \rightarrow 0$ , we use (2.4) to get

$$f_I(\lambda_I) = \lambda_I \frac{\int_{\mathbb{R}^N} w^{m-1} L_0^{-2} w^p dy}{\int_{\mathbb{R}^N} w^m dy} + O(\lambda_I^3) = \frac{\lambda_I}{p-1} \left[ \frac{1}{p-1} + \frac{1}{2m} \left( \frac{\int_0^\infty \rho^N (w^m)' d\rho}{\int_0^\infty \rho^{N-1} w^m d\rho} \right) \right] + O(\lambda_I^3). \quad (4.2 a)$$

Calculating the integral in (4.2 a) explicitly, and then substituting the result into (4.1 b) for  $g_I$ , we obtain

$$g_I = \frac{\lambda_I}{qm} [\tau - \tau_*] + O(\lambda_I^3), \quad \text{for } \lambda_I \ll 1, \quad (4.2 b)$$

where

$$\tau_* \equiv \frac{qm}{(p-1)} \left( \frac{1}{p-1} - \frac{N}{2m} \right). \quad (4.2 c)$$

This expression shows that  $f_I(0) < 0$  when  $p > 1 + 2m/N$ . By continuity, the inequality  $f_I < 0$  must hold on some interval near  $\lambda_I = 0$ . On this interval,  $g_I > 0$  for any  $\tau > 0$  when  $p > 1 + 2m/N$ . This suggests that for Type 2 data it is possible that  $\tau_0 < 0$ . More specifically,  $\tau_0 < 0$  if  $g_R = 0$  has a unique root at  $\lambda_I^0 > 0$  where  $f_I < 0$ .

The local behaviour of  $f_R$  as  $\lambda_I \rightarrow 0$  is more difficult to calculate. Using (2.4) and (4.1 a), we calculate

$$g_R = -\frac{\zeta}{qm} + \kappa_c \lambda_I^2 + O(\lambda_I^4), \quad \text{for } \lambda_I \ll 1, \quad (4.3 a)$$

where  $\zeta$  is defined in (1.2), and

$$\kappa_c \equiv \frac{1}{p-1} \frac{\int_{\mathbb{R}^N} w^{m-1} L_0^{-1} \left[ \frac{w}{p-1} + \frac{1}{2} \rho w' \right] dy}{\int_{\mathbb{R}^N} w^m dy}. \quad (4.3 b)$$

In general, the sign of  $\kappa_c$  is difficult to determine. There are two important cases where the sign of  $\kappa_c$  is known. When  $m = 2$ , the proof in §2 that  $f_R(\lambda_I)$  is monotone decreasing shows that we must have  $\kappa_c > 0$ . Next, suppose that  $m = p + 1$ . In this case, we can integrate by parts in (4.3 b) and then use (2.4) for  $L_0^{-1} w^p$  to evaluate the resulting expression. In this way, we obtain

$$\kappa_c = \frac{C_{N,p}}{(p-1)^2} \left[ \frac{1}{p-1} - \frac{N}{4} \right], \quad \text{for } m = p + 1, \quad (4.3 c)$$

where  $C_{N,p} > 0$  is defined in (2.30). Therefore,  $\kappa_c > 0$  if  $m = p + 1$  and  $1 < p < 1 + 4/N$ . Alternatively, when  $\kappa_c < 0$ , it follows that  $f_R$  is an increasing function for  $\lambda_I$  small.

If  $\tau < 0$ , the discussion leading to the formula (3.5) for the number of zeroes in the right half-plane requires modification. Assume that  $\tau$  is such that there are no zeroes on the imaginary axis. For  $\tau < 0$ , it is clear from the formula for  $g(\lambda)$  in (3.1) that the change in the argument of  $g$  over the semicircle  $\Gamma_R$  as  $R \rightarrow \infty$  is now  $-\pi$ . In place of (3.5), we then obtain the following formula for the number  $M$  of eigenvalues of (2.3) in the right half-plane  $\text{Re}(\lambda) > 0$ :

$$M = \frac{1}{2} + \frac{1}{\pi} \Delta_{\Gamma_I} g, \quad \text{where } \Delta_{\Gamma_I} g \equiv [\arg g]_{\Gamma_I}, \quad \tau < 0. \quad (4.4)$$

Again  $[\arg g]_{\Gamma_I}$  denotes the change in the argument of  $g$  along the semi-infinite imaginary axis  $\Gamma_I = i\lambda_I$ ,  $0 \leq \lambda_I < \infty$ , traversed in the downwards direction.

If we assume that  $g_R = 0$  has exactly one root, then the results obtained earlier for Type 1 data also largely apply to Type 2 data. The following lemma is a simple generalization of Lemma 3.1.

**Lemma 4.1:** *Suppose that there is exactly one root  $\lambda_I^0 > 0$  to  $g_R = 0$  on  $\lambda_I \geq 0$ , where  $g_R$  is defined in (4.1 a). Let  $\tau_0$  be the unique root to  $g_I = 0$  in (4.1 b). Then, if  $\tau_0 > 0$  and  $0 < \tau < \tau_0$ , there are no eigenvalues of (2.3) in the right half-plane. If  $\tau > \tau_0$  there are exactly two eigenvalues of (2.3) in the right half-plane.*

The proof is simple except that now we have to allow for the possibility that  $\tau_0 < 0$  and  $\tau < 0$ . Suppose first that  $\tau_0 > 0$ . Then the key properties of  $g_R$  and  $g_I$  needed in the proof of Lemma 3.1 still hold. Namely,

for any  $\tau > 0$ , we have  $g_R > 0$  and  $g_I > 0$  for  $\lambda_I$  sufficiently large, with  $g_I/g_R \rightarrow +\infty$  as  $\lambda_I \rightarrow \infty$ . Also,  $g_R < 0$  and  $g_I = 0$  at  $\lambda_I = 0$ , and  $g_I = (\tau - \tau_0)\lambda_I^0/(qm)$  at the unique point where  $g_R = 0$ . We then use the criterion (3.5) to conclude that  $M = 2$  and  $M = 0$  when  $\tau > \tau_0$  and  $0 < \tau < \tau_0$ , respectively. Suppose that  $\tau_0 < 0$ . If  $\tau_0 < 0 < \tau$ , the proof is contained above, so that  $M = 2$ . If  $\tau_0 < \tau < 0$ , then  $g_R > 0$  and  $g_I < 0$  for  $\lambda_I$  sufficiently large, with  $g_I/g_R \rightarrow -\infty$  as  $\lambda_I \rightarrow \infty$ . The other conditions on  $g_R$  and  $g_I$  are the same. Thus,  $\Delta_{\Gamma_I} g = \pi/2$ , and from (4.4) we get  $M = 2$ .

Under the key condition of Lemma 4.1, namely that  $g_R = 0$  has only one root on  $\lambda_I \geq 0$ , all of the qualitative features of the dependence of  $\lambda = \lambda_R + i\lambda_I$  on the parameter  $\tau$  must be precisely the same as for the case of Type 1 data discussed in §3.1. This condition on  $g_R$  is the monotonicity condition mentioned in §1. The complex conjugate pair of eigenvalues must merge onto the positive real axis when  $\tau = \tau_c$  where  $\lambda_R = \lambda_R^0 > 0$ . However, here it is possible that  $\tau_c \leq 0$ . In place of (3.8), for  $\tau > \tau_c$ , the two eigenvalues along the real axis satisfy

$$\tau = E(\lambda_R), \quad \text{where} \quad E(\lambda_R) \equiv \frac{1}{\lambda_R} [mqf_R(\lambda_R) - (s+1)], \quad (4.5 a)$$

and

$$f_R(\lambda_R) \equiv \frac{\int_{\mathbb{R}^N} w^{m-1} (L_0 - \lambda_R)^{-1} w^p dy}{\int_{\mathbb{R}^N} w^m dy}. \quad (4.5 b)$$

Since  $f_R(0) = 1/(p-1)$ , and  $L_0$  is unbounded as  $\lambda_R \rightarrow \nu_0^-$ , we have  $E \rightarrow +\infty$  as  $\lambda_R \rightarrow 0$  and  $E \rightarrow +\infty$  as  $\lambda_R \rightarrow \nu_0^-$ . The value  $\tau_c$  is obtained from the minimization condition

$$\tau_c = \min_{0 < \lambda_R < \nu_0} E(\lambda_R). \quad (4.5 c)$$

The sign of  $\tau_c$  depends on the data. Since, under the conditions of Lemma 4.1, there are only two eigenvalues in the right half-plane when  $\tau > \tau_0$ , and since  $E \rightarrow +\infty$  at the endpoints of the interval  $(0, \nu_0)$ , there must be exactly two roots to (4.5 a) for any  $\tau > \tau_c$ . This implies, indirectly, that  $E$  must have a global minimum, with no other local maxima or minima. Thus, once the complex conjugate pair of eigenvalues have merged onto the real axis, they can never leave the real axis for  $\tau > \tau_c$ . The asymptotic formulae (3.15) and (3.20) for the behaviour of the eigenvalues on the real axis as  $\tau \rightarrow \infty$  hold for any  $m > 1$ .

We now give some numerical results. For the exponent set  $(p, q, m, s) = (4, 2, 2, 0)$  we are guaranteed that, since  $m = 2$ ,  $g_R = 0$  has only one root. For the exponent set  $(p, q, m, s) = (3, 2, 3, 1)$ , we found numerically that  $g_R = 0$  has only one root for  $N = 1$ ,  $N = 2$ , and  $N = 3$ . The numerical values for  $\tau_0$ ,  $\lambda_I^0$ ,  $\tau_c$ ,  $\lambda_R^0$ , and  $\nu_0$ , accurate to the decimal places shown, are given in Table 3. For the exponent set  $(p, q, m, s) = (4, 2, 2, 0)$ , we see from this table that  $\tau_0 < 0$  for  $N = 2$  and  $N = 3$ . In addition,  $\tau_c > 0$  when  $N = 2$ , and  $\tau_c < 0$  when  $N = 3$ . This shows that when  $\tau = 0$ , the eigenvalue problem (2.3) for the exponent set  $(p, q, m, s) = (4, 2, 2, 0)$  has two positive real eigenvalues when  $N = 3$ , and a complex conjugate pair of eigenvalues with positive real parts when  $N = 2$ .

It is easy to combine the local behaviours (4.2) and (4.3) to recover a result of [20]. Let  $\zeta$  be as defined

$(p, q, m, s)$	$N$	$\tau_0$	$\lambda_I^0$	$\tau_c$	$\lambda_R^0$	$\nu_0$
(2, 1, 3, 0)	1	0.819	1.776	8.027	0.565	1.25
(2, 1, 3, 0)	2	0.631	2.362	6.184	0.751	1.65
(2, 1, 3, 0)	3	0.443	3.427	4.383	1.064	2.36
(3, 2, 3, 1)	1	0.666	2.121	2.488	1.100	3.00
(3, 2, 3, 1)	2	0.361	3.741	1.344	2.605	5.41
(3, 2, 3, 1)	3	0.122	9.241	0.415	5.551	15.29
(4, 2, 2, 0)	2	-0.0193	2.539	0.0931	3.674	13.23
(4, 2, 2, 0)	3	-0.323	1.291	-0.0838	2.655	144.18

Table 3. Numerical values for  $\tau_0$ ,  $\lambda_I^0$ ,  $\tau_c$ ,  $\lambda_R^0$ , and  $\nu_0$  for different Type 2 data.

in (1.2). The main results in [20] are obtained under the assumption that  $\zeta \rightarrow 0^+$ . Suppose, that  $\kappa_c > 0$  in (4.3 b). As remarked following (4.3 c), this condition is guaranteed to hold in two cases: (i)  $m = 2$ ; (ii)  $m = p + 1$  and  $1 < p < 1 + 4/N$ . When  $\kappa_c > 0$ , there is a root to  $g_R = 0$  in (4.3 a) with

$$\lambda_I^0 \sim (qm\kappa_c)^{-1/2} \zeta^{1/2} + O\left(\zeta^{3/2}\right), \quad \zeta \rightarrow 0^+. \quad (4.6)$$

Then, from (4.2 b),  $g_I = 0$  has a root near the origin when

$$\tau = \tau_* + O(\zeta), \quad \zeta \rightarrow 0^+, \quad (4.7)$$

where  $\tau_*$  is given in (4.2 c). From following the proof of Lemma 4.1, we conclude that a one-spike solution is unstable when  $\tau > \tau_* + O(\zeta)$ . This is the essence of Theorems B and C of [20] for the shadow system.

In conclusion, under the monotonicity condition that  $g_R = 0$  has only one root for  $\lambda_I \geq 0$ , the qualitative behaviour of the eigenvalues for (2.3) under Type 1 and Type 2 data for  $\tau > \tau_0$  is very similar. The key difference is that for Type 2 data,  $\tau_0$  and  $\tau_c$  could be negative. When  $\tau_0 < 0$ , a one-spike solution to (1.3) will be unstable when  $\tau = 0$ . Recall that Theorem 2.2 above (cf. [24]), which gives sufficient conditions for the stability of a spike solution to (1.3) when  $\tau = 0$ , does not apply to certain Type 2 data. Given an exponent set  $(p, q, m, s)$  with  $m \neq 2$  and dimension  $N$ , it is easy to verify numerically whether or not  $g_R = 0$  has only one root. Although we do not have a proof that  $g_R = 0$  has only one root whenever  $m \neq 2$ , we have been unable to construct a counter-example exhibiting a case where  $g_R = 0$  has more than one root. This is an open problem. If  $g_R = 0$  did have more than one root, then since  $f_R \rightarrow 0$  as  $\lambda_I \rightarrow \infty$  and  $g_R < 0$  at  $\lambda_I = 0$ , it follows that there would be an odd number of roots to  $g_R = 0$ , and hence an odd number of critical values  $\tau_0$  where a Hopf bifurcation occurs.

## 5 Numerical Simulations of Small and Large-Scale Oscillations

In this section we solve (1.3) numerically on a radially symmetric domain  $0 \leq r \leq 1$ . For  $\varepsilon \ll 1$ , a one-spike equilibrium solution to (1.3) on the unit ball in  $N$ -dimensions is centred at the origin  $r = 0$ . From (2.1), it

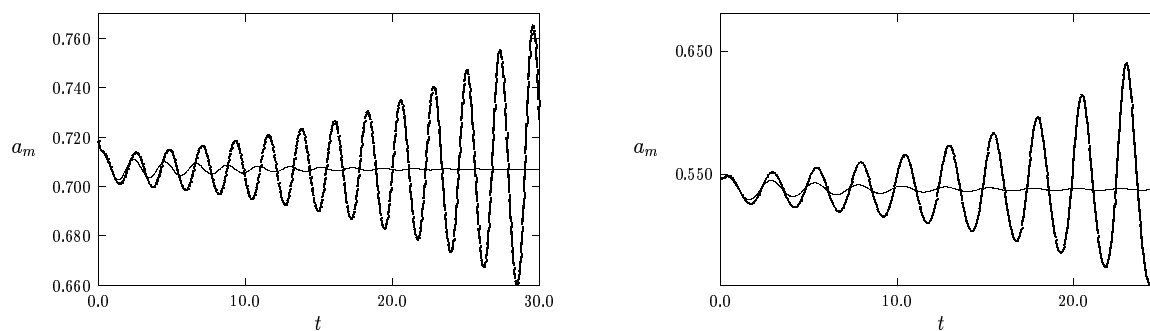
is given for  $\varepsilon \ll 1$  by

$$a_e(r) \sim h_e^\gamma w[\varepsilon^{-1}r], \quad h_e \sim \left[ (N-1) \int_0^\infty \rho^{N-1} [w(\rho)]^m d\rho \right]^{1/[1+s-\gamma m]}. \quad (5.1)$$

Here  $\gamma = q/(p-1)$ , and  $w$  is to be computed from (2.2). In each of the computational experiments below, we took the initial condition for (1.3) to be a localized perturbation of  $a_e$ . The initial condition is

$$a(r, 0) = \left[ 1 + 0.02e^{-r/\varepsilon} \cos\left(\frac{\pi r}{\varepsilon}\right) \right] a_e(r), \quad h(0) = h_e. \quad (5.2)$$

With this initial condition, (1.3) is solved numerically using the NAG library [17] for various exponent sets and dimensions  $N$ . The method of lines with 3000 meshpoints across the interval was used. The error tolerance in the time-stepping was very strict. In each of the computations below we took  $\varepsilon = 0.05$ . To illustrate the oscillatory behaviour we typically plot  $a_m \equiv a(0, t)$ , referred to as the amplitude of the spike, as a function of  $t$ .



(a)  $(p, q, m, s) = (3, 2, 2, 0)$  with  $N = 1$

(b)  $(p, q, m, s) = (4, 2, 2, 0)$  with  $N = 1$

FIGURE 8. Plots of  $a_m$  versus  $t$ . In the leftmost figure  $\tau = 0.28$  (solid curve) and  $\tau = 0.32$  (heavy solid curve). In the rightmost figure,  $\tau = 0.14$  (solid curve) and  $\tau = 0.155$  (heavy solid curve). For the left figure  $\tau_0 = 0.304$ , and for the right figure  $\tau_0 = 0.149$ .

We first give a partial confirmation of the Hopf bifurcation predicted in §3 and §4. For the exponent set  $(p, q, m, s) = (2, 1, 2, 0)$  with  $N = 2$ , in Fig. 1(a) of §1 we plot  $a_e$  and  $h_e$ , while in Fig. 1(b) we plot  $a_m$  versus  $t$ . From Fig. 1(b), we would anticipate that a Hopf bifurcation occurs somewhere in the range  $0.53 < \tau < 0.58$ . From Table 1, the theoretical value for the Hopf bifurcation is  $\tau_0 = 0.561$ . Similar plots can be done for other exponent sets. In particular, for  $N = 1$ , in Fig. 8(a) and Fig. 8(b) we plot  $a_m$  versus  $t$  for the exponent sets  $(p, q, m, s) = (3, 2, 2, 0)$  and  $(p, q, m, s) = (4, 2, 2, 0)$ , respectively. For each exponent set, the plots are shown for values of  $\tau$  on either side of the theoretical prediction for the Hopf bifurcation point  $\tau_0$ . From Table 1,  $\tau_0 = 0.304$  and  $\tau_0 = 0.149$  for Fig. 8(a) and Fig. 8(b), respectively. This numerical evidence suggests that the periodic solution initiated at  $\tau = \tau_0$  is unstable. It would be interesting to determine whether the Hopf bifurcation is subcritical or supercritical.

To illustrate the large-scale oscillatory dynamics under (1.3), we perform some numerical experiments at different values of  $\tau$  for the exponent set  $(p, q, m, s) = (2, 1, 2, 0)$  with  $N = 2$ . The form of the initial instability depends on the value of  $\tau$  in relation to the critical parameters  $\tau_0 = 0.561$  and  $\tau_c = 3.338$  given in Table 1 and Table 2, respectively. In Fig. 9(a) we show for  $\tau = 3.5 > \tau_c$  there are no oscillations, and  $a_m \rightarrow 0$  as  $t$  increases. However, when  $\tau = 2.8 < \tau_c$ , it is seen in Fig. 9(b) that the amplitude  $a_m$  has a dramatic peak, which is localized in time, before it decreases. The initial instability is oscillatory, but this feature is difficult to see from Fig. 9(b) owing to the large vertical scale. In Fig. 10(a), where we have taken  $\tau = 1.2$ , there is again a very large peak in the amplitude when  $t \approx 15.5$ , with  $a_m \rightarrow 0$  after the peak. For  $\tau = 1.2$ , the initial instability of the spike profile is oscillatory due to the complex conjugate eigenvalues of §3, and the oscillation precedes the occurrence of the peak.

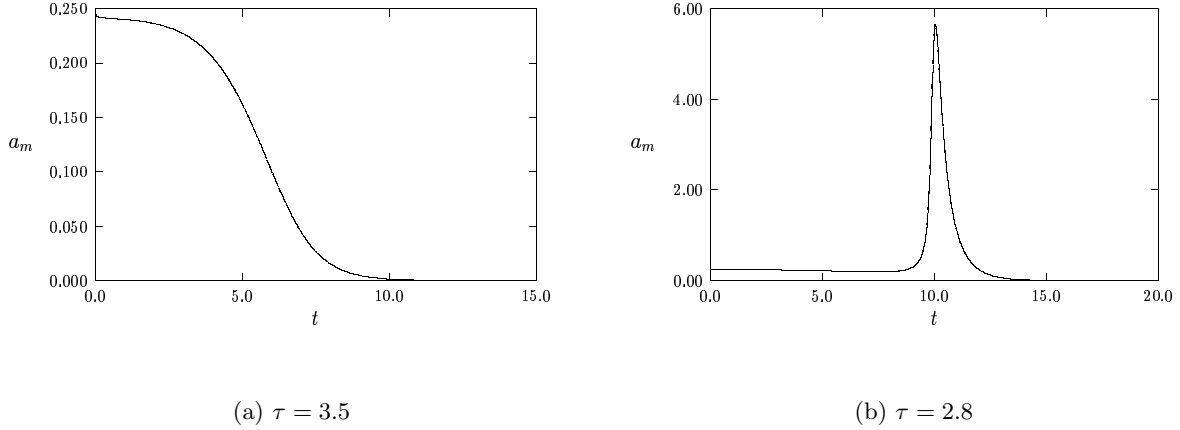


FIGURE 9. Plots of  $a_m$  versus  $t$  for  $(p, q, m, s) = (2, 1, 2, 0)$  and  $N = 2$ . For this data set  $\tau_0 = 0.561$ .

In an attempt to qualitatively explain these figures, it is convenient to make a change of variables in (1.3). Substituting  $a = h^\gamma v$  into (1.3), we obtain the following coupled problem for  $h$  and  $v$ :

$$v_t = \varepsilon^2 \Delta v - \left[ 1 + \gamma \frac{h_t}{h} \right] v + v^p, \quad x \in \Omega, \quad (5.3 a)$$

$$\tau \frac{h_t}{h} = -1 + \varepsilon^{-N} h^\zeta \int_{\Omega} v^m dx. \quad (5.3 b)$$

Here  $\zeta > 0$  is defined in (1.2), and  $\Omega$  is the unit ball in  $\mathbb{R}^N$ , with  $\partial_n v = 0$  on  $\partial\Omega$ . Notice that if  $v$  is localized, we have  $\varepsilon^{-N} \int_{\Omega} v^m dx = O(1)$  as  $\varepsilon \rightarrow 0$ . We define  $v_m$  by  $v_m \equiv v(0, t)$ . In order to compress the vertical scale, in Fig. 10(b) we plot  $\log_{10}(1 + v_m)$  and  $\log_{10}(1 + a_m)$  versus  $t$ .

To motivate the discussion below, we first consider the stability of spatially homogeneous equilibrium solutions of (5.3). Since  $\zeta > 0$  in (5.3 b), it is clear that the zero solution  $v \equiv 0$  and  $h \equiv 0$  is stable when  $\tau > \gamma$  and is unstable when  $0 \leq \tau < \gamma$ . Next, consider the nontrivial spatially homogeneous equilibrium

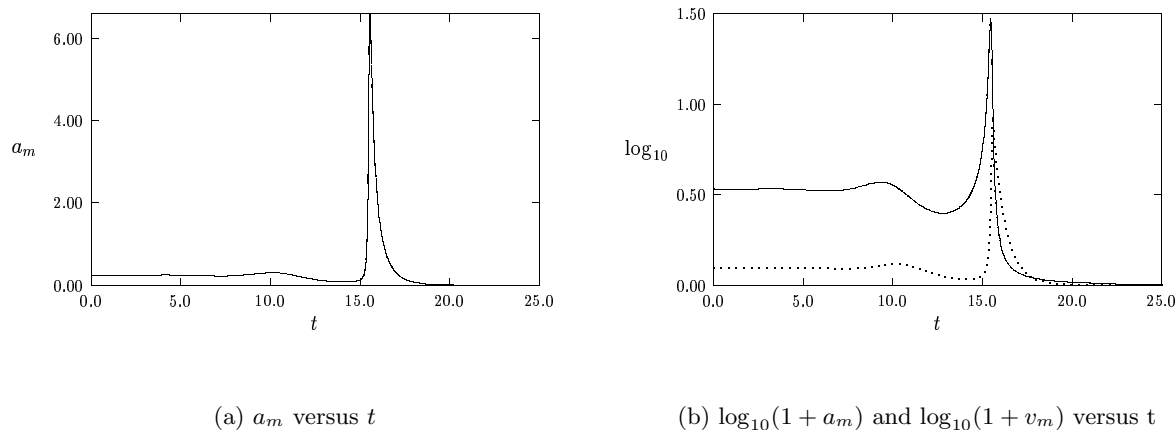


FIGURE 10. Plots of  $a_m$  versus  $t$  for  $(p, q, m, s) = (2, 1, 2, 0)$ ,  $N = 2$ , with  $\tau = 1.2$ . In the leftmost figure we plot  $a_m$  versus  $t$ , and in the rightmost figure we plot  $\log_{10}(1 + a_m)$  (dashed curve) and  $\log_{10}(1 + v_m)$  (solid curve) versus  $t$ . For this data set  $\tau_0 = 0.561$ .

solution  $v = v_u$  and  $h = h_u$ , given by

$$v_u = 1; \quad h_u = \left( \frac{\varepsilon^N}{|\Omega|} \right)^{1/\zeta}. \quad (5.4)$$

Substituting  $v = v_u + e^{\lambda t} \phi$  and  $h = h_u + e^{\lambda t} \eta$  into (5.3), where  $\phi \ll 1$  and  $\eta \ll 1$ , we obtain the eigenvalue problem

$$\varepsilon^2 \Delta \phi + (p-1)\phi = \lambda \phi + \frac{m\lambda\gamma}{\tau\lambda - \zeta} \frac{\int_{\Omega} \phi dx}{|\Omega|}, \quad (5.5)$$

with Neumann boundary conditions for  $\phi$ . If  $\int_{\Omega} \phi dx \neq 0$ , there is an eigenfunction  $\phi = c$ , where  $c$  is a constant. The corresponding eigenvalue  $\lambda_0$  satisfies,

$$\frac{\tau}{p-1} \lambda_0^2 + \lambda_0 \left[ \frac{s+1}{p-1} - \tau \right] + \zeta = 0. \quad (5.6)$$

Since  $\zeta > 0$ ,  $\text{Re}(\lambda_0) < 0$  only when  $0 \leq \tau < (s+1)/(p-1)$ . This condition on  $\tau$  is precisely the criterion for the stability of spatially homogeneous steady-states of (1.1) in the absence of any diffusion ( $\varepsilon = 0$  and  $D = 0$  in (1.1)). Next, suppose that  $\int_{\Omega} \phi dx = 0$ . Then, the corresponding eigenvalues are  $\lambda_j = (p-1) - \varepsilon^2 z_j^2$ , where  $z_j > 0$  for  $j \geq 1$  are the eigenvalues of the Laplacian. Hence, for  $\varepsilon \ll 1$ ,  $\lambda_j > 0$ . Therefore,  $v_u$  and  $h_u$  is always unstable for any  $\tau \geq 0$ . Thus, of the class of spatially uniform solutions, only the zero solution is stable when  $\tau > \tau_s \equiv \gamma$ . For  $(p, q, m, s) = (2, 1, 2, 0)$ , we have  $\tau_s = 1$ .

We now give a very rough idea of the mechanism for the sudden peak formations in  $a_m$ . In Fig. 10(b) we notice that  $v_m$  has a sharp increase before the dramatic peak in  $a_m$ . Suppose that  $v = O(1)$  in (5.3), with  $h$  sufficiently small so that  $h_t/h \approx -1/\tau$ . Then, since  $v = O(1)$ , the  $v^p$  term in (5.3 a) will result in a dramatic increase in  $v_m$ . If  $v$  was spatially uniform as in (5.4), the local growth rate would be  $\lambda \approx (p-1)$  as discussed in the previous paragraph. The instability here should be qualitatively similar. However, the

dramatic increase in  $v$  is self-limiting, since when  $v$  is too large the integral term in (5.3 *b*) dominates and  $h_t/h$  becomes strongly positive. A strongly negative coefficient for the linear  $v$  term in (5.3 *a*) then dominates the  $v^p$  term, allowing  $v$  to decrease.

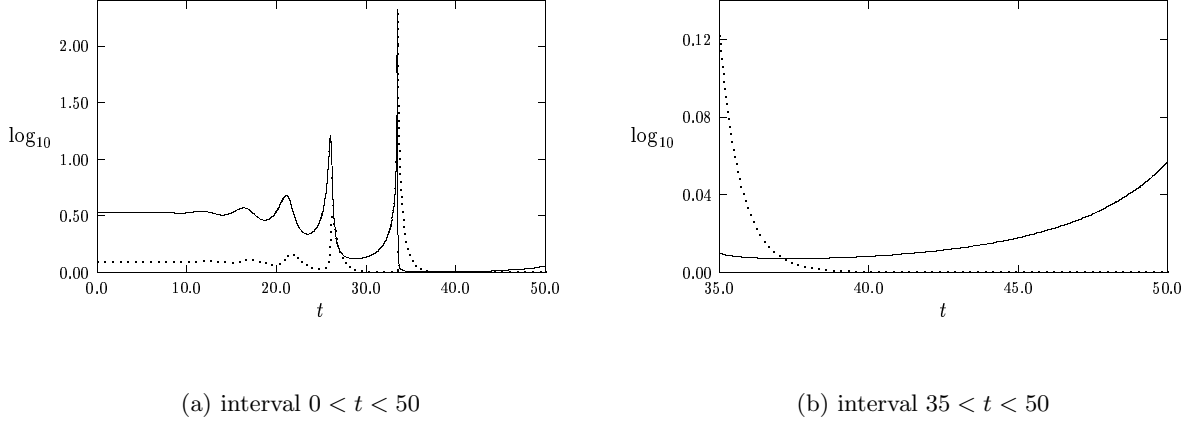


FIGURE 11. Plots of  $\log_{10}(1+a_m)$  (dashed curve) and  $\log_{10}(1+v_m)$  (solid curve) versus  $t$  for  $(p, q, m, s) = (2, 1, 2, 0)$ ,  $N = 2$ , with  $\tau = 0.8$ . In the rightmost figure our plot is only over the range  $35 < t < 50$  (after the peak in  $a_m$ ). Notice that  $v_m$  starts increasing even after the peak. For this data set  $\tau_0 = 0.561$ .

In Fig. 11(a) we plot  $\log_{10}(1+a_m)$  and  $\log_{10}(1+v_m)$  for the case  $\tau = 0.8$ . The initial instability is oscillatory since  $\tau_0 < \tau < \tau_c$ . In this case, on the interval  $0 \leq t < 50$ ,  $a_m$  has two pronounced peaks. As in Fig. 10(b),  $v_m$  has a sharp increase before each peak of  $a_m$ . In Fig. 11(b), where we plot the data in Fig. 11(a) only on the interval  $t > 35$ , we show that  $v_m$  first decreases after the second peak, but then starts increasing yet again. This is because the zero solution  $v \equiv 0$  is only stable when  $\tau > \tau_s = 1$ . Alternatively, for the case  $\tau = 3.5$ ,  $\tau = 2.8$ , and  $\tau = 1.2$  in Fig. 9(a), Fig. 9(b), and Fig. 10(a), respectively, we have verified numerically that  $v_m \rightarrow 0$  as  $t \rightarrow \infty$ . However, when  $\tau = 0.8$ , there are no stable spatially homogeneous steady-state solutions and the equilibrium one-spike solution at the origin is unstable. For this value of  $\tau$ , it is unclear what the global attractor is for the dynamics. We might expect some type of large-scale oscillatory motion that persists in time.

Similar type of small-scale scale oscillations for  $\tau \approx \tau_c$  and large-scale behaviour for  $\tau_c < \tau < \tau_s$  occur for other parameter sets. Consider now the case  $N = 1$  for the same exponent set  $(p, q, m, s) = (2, 1, 2, 0)$ . For this data set,  $\tau_0 = 0.771$ ,  $\tau_s = 1$ , and  $\tau_c = 4.560$  (see Table 1 and Table 2). In Fig. 12(a) we show that small-scale oscillations grow when  $\tau = 0.8$  and decrease when  $\tau = 0.75$ . In Fig. 12(b), where  $\tau = 0.95$ , we have a large-scale oscillatory motion in the spike amplitude  $a_m$ . For  $\tau = 0.95$ , the uniform solution  $v \equiv 0$  is unstable. In Fig. 13(a), where  $\tau = 1.5$ , small-scale oscillations precede one dramatic peak in  $a_m$ , with  $v_m \rightarrow 0$  after the peak. In Fig. 12(b) and Fig. 13(a), the plots are done on a logarithmic scale. In contrast,

in Fig. 13(b), we plot  $a_m$  versus  $t$  for  $\tau = 5.0$ . Since  $\tau > \tau_c$ , the initial instability is not oscillatory. After a very small peak in  $a_m$ , the amplitude  $a_m$  decreases to zero as  $t$  increases.

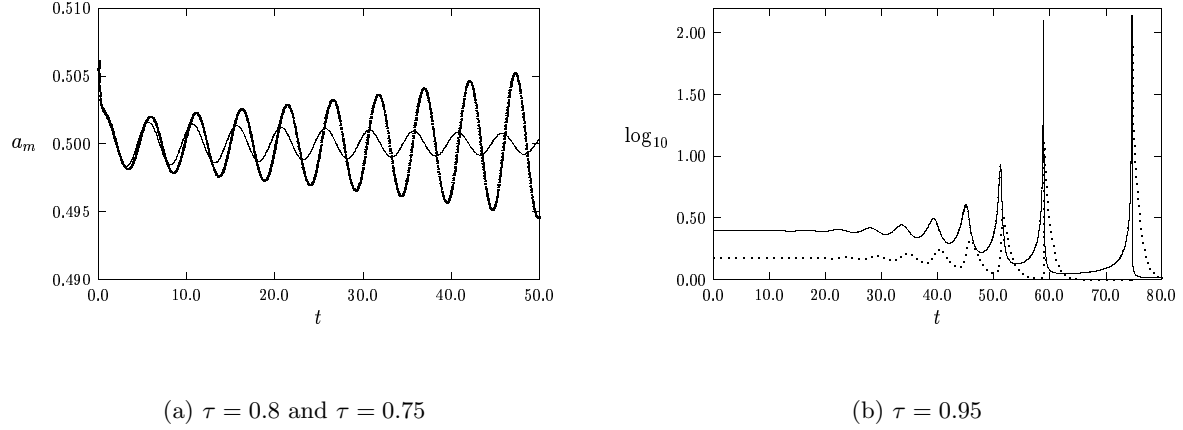


FIGURE 12. In the leftmost figure we plot  $a_m$  versus  $t$  for  $\tau = 0.75$  (solid curve) and  $\tau = 0.8$  (heavy solid curve). In the rightmost figure we plot  $\log_{10}(1 + a_m)$  (dashed curve) and  $\log_{10}(1 + v_m)$  (solid curve) versus  $t$  for  $\tau = 0.95$ . The parameters are  $(p, q, m, s) = (2, 1, 2, 0)$  and  $N = 1$ , for which  $\tau_0 = 0.771$ .

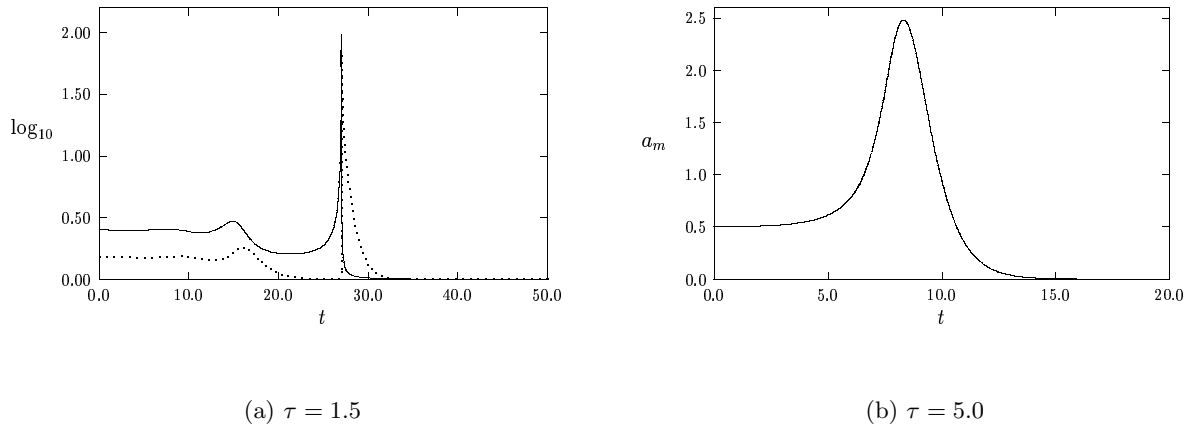


FIGURE 13. In the leftmost figure we plot  $\log_{10}(1 + a_m)$  (dashed curve) and  $\log_{10}(1 + v_m)$  (solid curve) versus  $t$  for  $\tau = 1.5$ . In the rightmost figure we plot  $a_m$  versus  $t$  for  $\tau = 5.0$ . The parameters are  $(p, q, m, s) = (2, 1, 2, 0)$  and  $N = 1$ , for which  $\tau_0 = 0.771$ .

## 6 Conclusions

In this paper we have analyzed the onset of oscillatory instabilities for a one-spike solution to (1.3) as a function of the reaction-time constant  $\tau$ , the dimension  $N$ , and the exponent set  $(p, q, m, s)$ . For Type 1

data, where  $m = 2$  and  $1 < p \leq 1 + 4/N$ , we have given a precise theoretical characterization of the spectrum of the linearized problem, and we have used numerical methods to compute the Hopf bifurcation values accurately. For Type 2 data, where  $m \neq 2$  or  $p > 1 + 4/N$ , our numerical results indicate a similar bifurcation behaviour. However, our theoretical results for Type 2 data are weaker than for data of Type 1.

In particular, a key open problem for Type 2 data is to prove a strict transversal crossing condition that states that a complex conjugate pair of eigenvalues can only cross from the left to the right half-plane as  $\tau$  increases. Such a condition, which is certainly suggested by our numerical results, would guarantee theoretically that there are exactly two eigenvalues in the right half-plane for any  $\tau > \tau_0$ . Our results in §3 have proved such a transversal crossing condition for Type 1 data.

Another open problem, for either Type 1 or Type 2 data, is to analyze the local behaviour near the Hopf bifurcation point to determine whether the bifurcating branch is subcritical or supercritical.

In §5 we gave a very rough idea of the qualitative features associated with large-scale dynamics, well beyond the onset of the instability, under the shadow GM model (1.3). An interesting open problem is to characterize precisely the large-scale oscillatory motion observed in the range  $\tau_0 < \tau < \tau_s = q/(p-1)$ , where both the spike and the zero solution are linearly unstable. A precise analysis of the stability of the degenerate zero solution would also be of interest. Finally, an extension of our basic approach could possibly be used to analyze oscillatory spike dynamics associated with the full GM model (1.1) with a finite  $D$ . For the one-dimensional case, such stability results are given in [23].

### Acknowledgements

J. W. thanks the support of RGC of Hong Kong and a direct grant from CUHK. M. J. W. thanks NSERC and the IMS of the Chinese University of Hong Kong, where this paper was written. The use of the computer facilities at the University of Washington Applied Math group is gratefully acknowledged.

### Appendix A The Proof of Lemma 2.4 of §2

In this appendix, we prove Lemma 2.4. Although this has been proved in Lemma 5.1 of [24], we include a proof here for the convenience of the readers.

We first assume that the strict inequality  $1 < p < 1 + 4/N$  holds. Let  $v$  be any real function with  $v \in \mathcal{H}^1(\mathbb{R}^N)$ . Define the operator  $L_1$  by

$$\begin{aligned} L_1 v \equiv & L_0 v - (p-1) \left( \frac{\int_{\mathbb{R}^N} wv \, dy}{\int_{\mathbb{R}^N} w^2 \, dy} \right) w^p - (p-1) \left( \frac{\int_{\mathbb{R}^N} w^p v \, dy}{\int_{\mathbb{R}^N} w^2 \, dy} \right) w \\ & + (p-1) \frac{\left( \int_{\mathbb{R}^N} w^{p+1} \, dy \right) \left( \int_{\mathbb{R}^N} wv \, dy \right)}{\left( \int_{\mathbb{R}^N} w^2 \, dy \right)^2} w. \end{aligned} \tag{A.1}$$

Here  $L_0$  is defined in (2.3 c). The operator  $L_1$  is clearly self-adjoint. Denote the kernel of  $L_1$  by  $X_1$ . In the

first part of Lemma 5.1 of [24], it was proved that

$$X_1 = \text{span}\left\{w; \frac{\partial w}{\partial y_j}, j = 1, \dots, N\right\}. \quad (\text{A.2})$$

Lemma 2.4 of §2 reduces to showing that  $\int_{\mathbb{R}^N} v L_1 v \, dy \leq 0$  for any  $v \in \mathcal{H}^1(\mathbb{R}^N)$ .

We proceed by contradiction. Suppose Lemma 2.4 is false. Then, there exists a pair  $(\alpha, \phi)$  such that: (i)  $\alpha$  is real and positive; (ii)  $\phi \perp X_1$ ; (iii)  $L_1 \phi = \alpha \phi$ . We show that this is impossible. From (ii), (iii), and (A.1), we have

$$(L_0 - \alpha) \phi = (p - 1) \left( \frac{\int_{\mathbb{R}^N} w^p \phi \, dy}{\int_{\mathbb{R}^N} w^2 \, dy} \right) w. \quad (\text{A.3})$$

We first claim that  $\int_{\mathbb{R}^N} w^p \phi \, dy \neq 0$ . In fact, if  $\int_{\mathbb{R}^N} w^p \phi \, dy = 0$ , then  $\alpha > 0$  is an eigenvalue of  $L_0$ . However, by Theorem 2.12 of [14], written in §2 as Theorem 2.1, there is only one positive eigenvalue of  $L_0$ , labeled by  $\nu_0$ , and the corresponding eigenfunction is radially symmetric and has one sign. This contradicts that  $\phi \perp X_1$ . Therefore,  $L_0 - \alpha$  is invertible in  $X_1^\perp$ , and from (A.3)

$$\phi = (p - 1) \left( \frac{\int_{\mathbb{R}^N} w^p \phi \, dy}{\int_{\mathbb{R}^N} w^2 \, dy} \right) (L_0 - \alpha)^{-1} w. \quad (\text{A.4})$$

Multiplying (A.4) by  $w^p$  and integrating, we get

$$\int_{\mathbb{R}^N} w^p \phi \, dy = (p - 1) \left( \frac{\int_{\mathbb{R}^N} w^p \phi \, dy}{\int_{\mathbb{R}^N} w^2 \, dy} \right) \int_{\mathbb{R}^N} [(L_0 - \alpha)^{-1} w] w^p \, dy. \quad (\text{A.5})$$

In (A.5) we use  $L_0 w = (p - 1)w^p$ , and cancel the common factor, to obtain

$$\int_{\mathbb{R}^N} w^2 \, dy = (p - 1) \int_{\mathbb{R}^N} [(L_0 - \alpha)^{-1} w] w^p \, dy = \int_{\mathbb{R}^N} [(L_0 - \alpha)^{-1} w] [(L_0 - \alpha) w + \alpha w] \, dy. \quad (\text{A.6})$$

We then integrate by parts in (A.6) to get

$$0 = \int_{\mathbb{R}^N} [(L_0 - \alpha)^{-1} w] w \, dy. \quad (\text{A.7})$$

Define  $h_1(\alpha) \equiv \int_{\mathbb{R}^N} [(L_0 - \alpha)^{-1} w] w \, dy$  to be the right-hand side of (A.7). The contradiction is established by showing that  $h_1(\alpha)$  cannot vanish.

Set  $\alpha = 0$  to get  $h_1(0) = \int_{\mathbb{R}^N} (L_0^{-1} w) w \, dy$ . Using (2.4) for  $L_0^{-1} w$ , we integrate the resulting expression for  $h_1(0)$  by parts, to get

$$h_1(0) = \left( \frac{1}{p-1} - \frac{N}{4} \right) \int_{\mathbb{R}^N} w^2 \, dy > 0, \quad (\text{A.8})$$

since  $1 < p < 1 + 4/N$ . Moreover,  $h'_1(\alpha) = \int_{\mathbb{R}^N} [(L_0 - \alpha)^{-2} w] w \, dy = \int_{\mathbb{R}^N} [(L_0 - \alpha)^{-1} w]^2 \, dy > 0$ . This inequality and (A.8) proves that  $h_1(\alpha) > 0$  for all  $\alpha \in (0, \nu_0)$ . Since  $\lim_{\alpha \rightarrow +\infty} h_1(\alpha) = 0$ , and  $h'_1(\alpha) > 0$ , it follows that  $h_1(\alpha) < 0$  for all  $\alpha \in (\nu_0, \infty)$ . The fact that  $h_1(\alpha)$  is never zero is a contradiction to (A.7). Hence, when  $1 < p < 1 + 4/N$ ,  $\int_{\mathbb{R}^N} v L_1 v \leq 0$  for any  $v \in \mathcal{H}^1(\mathbb{R}^N)$ . This completes the proof of Lemma 2.4 of §2 when  $1 < p < 1 + 4/N$ .

The proof for the borderline case when  $m = 2$  and  $p = 1 + 4/N$  requires only a little modification. We

again must show that  $\int_{\mathbb{R}^N} v L_1 v \leq 0$  for any  $v \in \mathcal{H}^1(\mathbb{R}^N)$ . However, in this case, it was shown in Lemma 5.2 of [24] that the span  $X_1$  of  $L_1$  is now

$$X_1 = \text{span}\left\{w; w_0; \frac{\partial w}{\partial y_j}, j = 1, \dots, N\right\}, \quad (\text{A.9})$$

where

$$w_0 \equiv \frac{w}{p-1} + \frac{1}{2}y \cdot \nabla w. \quad (\text{A.10})$$

We can repeat the steps from (A.3)–(A.8), but this time conclude that  $h_1(0) = 0$ , and  $h_1'(\alpha) < 0$  for  $\alpha \geq 0$ . There is still however no positive root to  $h_1(\alpha) = 0$ . This is a contradiction, and so Lemma 2.4 of §2 is proved in the borderline case  $m = 2$ ,  $p = 1 + 4/N$ .

### Appendix B Calculation of an Integral in §2

Here we show how to obtain (2.30). This is done by obtaining a linear system for the two integrals  $e$  and  $b$  defined by

$$e = \frac{\int_0^\infty \rho^{N-1} w^{p+1} d\rho}{\int_0^\infty \rho^{N-1} w^2 d\rho}, \quad b = \frac{\int_0^\infty \rho^{N-1} (w')^2 d\rho}{\int_0^\infty \rho^{N-1} w^2 d\rho}. \quad (\text{B.1})$$

The resulting formula for  $e$  will yield (2.30).

We begin by writing (2.2 a) for  $w$  as

$$\left[\rho^{N-1} w'\right]' - \rho^{N-1} w + \rho^{N-1} w^p = 0. \quad (\text{B.2})$$

Multiplying (B.2) by  $w$ , and integrating by parts, we get one equation

$$e = 1 + b. \quad (\text{B.3})$$

The second equation is obtained from multiplying (B.2) by  $\rho w'$  and integrating the resulting expression by parts. This gives,

$$(N-2)b + N - \frac{2N}{p+1}e = 0. \quad (\text{B.4})$$

Solving (B.3) and (B.4) for  $e$  we get the result in (2.30),

$$e = \frac{p+1}{N+(p+1)(1-N/2)}. \quad (\text{B.5})$$

### References

- [1] U. Ascher, R. Christiansen, R. Russell, *Collocation Software for Boundary Value ODE's*, Math. Comp., **33**, (1979), pp. 659-679.
- [2] P. Bates, N. Fusco, *Equilibria with Many Nuclei for the Cahn-Hilliard Equation*, J. Diff. Eq. **160**, No. 2, (2000), pp. 283-356.
- [3] X. Chen, M. Kowalczyk, *Slow Dynamics of Interior Spikes in the Shadow Gierer-Meinhardt System*, Adv. in Diff. Equat., **6**, No. 7, (2001), pp. 847-872.
- [4] E. N. Dancer, *On Stability and Hopf Bifurcations for Chemotaxis Systems*, Methods and Appl. of Analysis, Vol. 8, No. 2, (2001), pp. 245-256.

- [5] A. Doelman, T. J. Kaper, P. Zegeling, *Pattern Formation in the One-Dimensional Gray-Scott Model*, *Nonlinearity*, **10**, (1997), pp. 523-563.
- [6] A. Doelman, R. A. Gardner, T. J. Kaper, *Stability Analysis of Singular Patterns in the 1D Gray-Scott Model: A Matched Asymptotics Approach*, *Physica D*, **122**, (1998), pp. 1-36.
- [7] A. Doelman, R. A. Gardner, T. Kaper, *A Stability Index Analysis of 1-D Patterns of the Gray Scott Model*, *Memoirs of the AMS*, **155**, No. 737, (2002).
- [8] A. Gierer, H. Meinhardt, *A Theory of Biological Pattern Formation*, *Kybernetik*, **12**, (1972), pp. 30-39.
- [9] C. Gui, J. Wei, *Multiple Interior Peak Solutions for Some Singularly Perturbed Neumann Problems*, *J. Diff. Eq.*, No. 1 Vol. **158**, (1999), pp. 1-27.
- [10] L. Harrison, D. Holloway, *Order and Localization in Reaction-Diffusion Pattern*, *Physica A*, **222**, (1995), pp. 210-233.
- [11] D. Iron, M. J. Ward, *A Metastable Spike Solution for a Non-Local Reaction-Diffusion Model*, *SIAM J. Appl. Math.*, **60**, No. 3, (2000), pp. 778-802.
- [12] D. Iron, M. J. Ward, *The Dynamics of Boundary Spikes for a Non-Local Reaction-Diffusion Model*, *Europ. J. Appl. Math.*, **11**, No. 5, (2000), pp. 491-514.
- [13] M. Kowalczyk, *Multiple Spike Layers in the Shadow Gierer-Meinhardt System: Existence of Equilibria and Approximate Invariant Manifold*, *Duke Math J.*, **98**, No. 1, (1999), pp. 59-111.
- [14] C. S. Lin, W. M. Ni, I. Takagi, *Large Amplitude Stationary Solutions to a Chemotaxis System*, *J. Diff. Eq.*, **72**, (1988), pp. 1-27.
- [15] H. Meinhardt, *Models of Biological Pattern Formation*, Academic Press, London, (1982).
- [16] H. Meinhardt, *The Algorithmic Beauty of Sea Shells*, Springer-Verlag, Berlin, (1995).
- [17] NAG Fortran library Mark 17, routine D03PCF, Numerical Algorithms Group Ltd., Oxford, United Kingdom (1995).
- [18] W. Ni, *Diffusion, Cross-Diffusion, and Their Spike-Layer Steady-States*, *Notices of the AMS*, Vol. **45**, No. 1, (1998), pp. 9-18.
- [19] W. M. Ni, I. Takagi, *Locating the Peaks of Least Energy Solutions to a Singularly Perturbed Neumann Problem*, *Duke Math J.*, **70**, (1993), pp. 247-281.
- [20] W. Ni, I. Takagi, E. Yanagida, *Stability Analysis of Point-Condensation Solutions to a Reaction-Diffusion System Proposed by Gierer and Meinhardt*, to appear, *Tohoku Math J.*, (2002).
- [21] A. Turing, *The Chemical Basis of Morphogenesis*, *Phil. Trans. Roy. Soc. B*, **327**, (1952), pp. 37-72.
- [22] M. J. Ward, *An Asymptotic Analysis of Localized Solutions for Some Reaction-Diffusion Models in Multi-Dimensional Domains*, *Stud. Appl. Math.*, **97**, No. 2, (1996), pp. 103-126.
- [23] M. J. Ward, J. Wei, *Hopf Bifurcations and Oscillatory Instabilities of Spike Solutions for the One-Dimensional Gierer-Meinhardt Model*, *J. Nonlinear Science*, to appear, (2003), (58 pages).
- [24] J. Wei, *On Single Interior Spike Solutions for the Gierer-Meinhardt System: Uniqueness and Stability Estimates*, *Europ. J. Appl. Math.*, Vol. **10**, No. 4, (1999), pp. 353-378.
- [25] J. Wei, *On the Interior Spike Layer Solutions to a Singularly Perturbed Neumann Problem*, *Tohoku Math. J.*, **50**, (1998), pp. 159-178.